

AFIT/GAP/ENP/95D-14

**IDENTIFICATION OF MOLECULAR
LASER TRANSITIONS
USING THE FINITE ELEMENT METHOD**

THESIS

Matthew C. Smitham, Captain, USAF

AFIT/GAP/ENP/95D-14

Approved for public release; distribution unlimited

1996 0118 031

DTIC QUALITY INSPECTED 3

“The views expressed in this thesis/dissertation are those of the author(s) and do reflect the official policy or position of the Department of Defense.”

AFIT/GAP/ENP/95D-14

**IDENTIFICATION OF MOLECULAR LASER TRANSITIONS USING THE
FINITE ELEMENT METHOD**

THESIS

**Presented of the Faculty of the School of Engineering
of the Air Force Institute of Technology
Air University in Partial Fulfillment of the
Requirements for the Degree of
Master of Science in Engineering Physics**

**Matthew C. Smitham, B.S.,
Captain, USAF**

December 1995

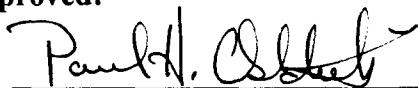
Approved for public release; distribution unlimited

IDENTIFICATION OF MOLECULAR LASER TRANSITIONS USING THE
FINITE ELEMENT METHOD

Matthew C. Smitham, B.S.,
Captain, USAF

THESIS

Approved:



Paul H. Ostdiek, Lieutenant Colonel, USAF
Chairman, Advisory Committee

15 Nov 95



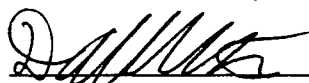
David L. Coulliette, Major, USAF
Member, Advisory Committee

15 Nov 95



Glen P. Perram, Major, USAF
Member, Advisory Committee

15 Nov 95



David E. Weeks
Member, Advisory Committee

14 Nov 95



Ernest A. Dorko
Member, Advisory Committee

3 DEC 95

Acknowledgments

I am indebted to my thesis advisor, Lt Col Paul H. Ostdiek, for his insight, guidance, and encouragement throughout this thesis project. I am especially grateful for his selfless gift of time and energy when I frequently presented myself unannounced at his office door with an endless list of questions and frustrations. Time and again, his answers motivated me to learn more about the problem at hand, and refocused my efforts back onto the defined objective.

I would also like to thank the members of my committee. Thanks to Maj Coulliette for helping me to garner a much deeper understanding of the method of finite elements, and to Dr Weeks for his quantum mechanical insights, especially for his help with the hydrogen molecule. And, I would like to also thank Maj Perram for his insights into molecular spectroscopy, and Dr Dorko for his advice and background material.

I am eternally grateful to Dr William F. Bailey for his faith in my abilities. Without Dr Bailey, my AFIT experience would never have happened.

And finally, but certainly not least, I would like to thank my wife, Kymberly, for her support during this past year and a half. Not only did she put off her own career aspirations so I could attend AFIT, but tolerated my long hours away at work or locked in the study. To her, I dedicate this thesis.

Matthew C. Smitham

Table of Contents

	<u>Page</u>
Acknowledgements.....	ii
List of Figures.....	v
Abstract.....	vii
I. Introduction.....	I-1
Background.....	I-1
Objectives.....	I-5
Scope.....	I-5
Approach.....	I-6
II. Literature Background and Theory.....	II-1
Introduction.....	II-1
Laser Transitions.....	II-2
Diatomic Molecules.....	II-9
Franck-Condon Principle.....	II-19
Numerical Solution of Schrödinger's Equation.....	II-23
Conclusion.....	II-33
III. Computer Modeling and Programs.....	III-1
Introduction.....	III-1
Background of Computer Models.....	III-2
Preparation of Spectroscopic Data.....	III-5
The Hunt.....	III-10
Franck-Condon Calculations.....	III-26
IV. Validation.....	IV-1
Introduction.....	IV-1
Simple Harmonic Oscillator.....	IV-1
The Morse Anharmonic Oscillator.....	IV-7

	Convergence.....	IV-12
	Hydrogen Molecule.....	IV-21
	Conclusion.....	IV-25
V.	Conclusion.....	V-1
	Summary.....	V-1
	Recommendations.....	V-3
	Bibliography.....	BIB 1
	Vita.....	Vita 1

List of Figures

<u>Figure</u>	<u>Page</u>
II-1 Schematic Diagram of Laser.....	II-3
II-2 Intermolecular Force Model.....	II-12
II-3 Harmonic Eigenfunctions.....	II-14
II-4 Morse Oscillator.....	II-16
II-5 Morse Eigenfunctions.....	II-18
II-6 Franck-Condon Principle.....	II-21
II-7 Finite Element Grid.....	II-26
II-8 Building the Global Matrix.....	II-30
III-1 Dunham Input File.....	III-6
III-2 Molecular Transitions.....	III-8
III-3 Efit Input File.....	III-9
III-4 The Hunting Process.....	III-14
III-5 The Parameter Space.....	III-16
III-6 Diatom Energy Input File.....	III-19
III-7 Diatom Control Input File.....	III-20
IV-1 Comparisons of Simple Harmonic Oscillator Eigenfunctions (0,1).....	IV-5
IV-2 Comparisons of Simple Harmonic Oscillator Eigenfunctions (6,9).....	IV-6
IV-3 Comparisons of Morse Eigenfunctions (0,1).....	IV-10

IV-4	Comparisons of Morse Eigenfunctions (6,9).....	IV-11
IV-5	Convergence of Simple Harmonic Oscillator.....	IV-13
IV-6	Divergence of Morse Solution.....	IV-14
IV-7	Convergence of Morse Solution.....	IV-16
IV-8	Divergence as Function of Left Grid Point Position.....	IV-17
IV-9	Convergence Rate.....	IV-18
IV-10	Execution Time.....	IV-20
IV-11	Hydrogen Molecule Potential Curve Comparison.....	IV-23

Abstract

This thesis is a continuation of a previous effort which developed a finite element solution of Schrödinger's Equation. The purpose of this research is to extend this previous work, and develop a chemical laser engineering tool for the identification of transition lines. Identification of laser transitions for a new chemical gain medium requires knowledge of Einstein's Coefficients. These transitions rates can be obtained by solving Schrödinger's Equation for diatomic molecules using the method of finite elements. Experimental vibrational eigenvalues for a given electronic state are used to determine the molecular potential surface which yields the closest numerical result. A non-linear minimization routine is used to hunt for this surface by adjusting parameters of energy functions such as the Harmonic, Morse, Lennard-Jones, and Mie potentials. For each set of new parameters selected by the minimization routine, the method of finite elements is used to solve Schrödinger's Equation. The eigenvalues from these solutions are then compared to the experimental values. Through this iterative process, the best potential surface is isolated. Franck-Condon factors, which are proportional to Einstein's coefficients, can be computed with the numerical eigenfunctions from two different potential surfaces found in this way.

This numerical technique was able to isolate potential surfaces whose eigenvalue solutions had relative errors better than 10^{-3} and 10^{-6} percent when compared to the analytical solutions of the Harmonic and Morse oscillators, respectively. Comparisons of the wavefunctions also yielded excellent agreement. Initial work with $H_2 (X^1\Sigma_g^+)$ verifies the lower eigenstates can be approximated by the Morse potential with an anharmonicity term of 1.0912 inverse a.u. and a dissociation energy of 0.177 Hartrees.

IDENTIFICATION OF MOLECULAR LASER TRANSITIONS USING THE FINITE ELEMENT METHOD

I .Introduction

Background

The Air Force has on-going research to develop new and/or better battlefield laser weapon systems which will prove powerful and economical in the field. This thesis research project contributes to this effort by aiding the identification of molecular candidates for chemical laser systems in a cheap and effective manner. Military applications of these laser systems include countermeasures against infrared guided missiles, theater defense, weapons guidance, and other battlefield applications.

To determine whether a molecule is a good candidate for lasing, the molecule's energy transition rates must be understood. These transition rates, calculated using Einstein's Coefficients, identify if a sufficient population inversion can be achieved to establish lasing between two energy levels of an atom or molecule (1:179-183,616-624). Often, this data is not available or incomplete leaving the researcher unable to analyze the molecule for its lasing potential. At this point, the investigator must endeavor in a time

consuming and possibly expensive laboratory research to obtain this data, and then evaluate the molecule as a lasing candidate.

However, Franck-Condon probability factors which are related to these transition rates can be obtained through theoretical calculations if sufficient spectroscopic data is available. Commonly, molecular spectroscopists use the semi-classical Rydberg-Klein-Rees (RKR) method with an Inverted Perturbation Approach (IPA) refinement for these calculations. The Air Force Institute of Technology in the early 1980's (2; 3; 4) used a RKR-IPA model developed by Vidal and Scheingraber (5) as a research tool for previous work related to this thesis.

The RKR method uses constants experimentally derived from spectroscopic data to calculate the classical turning points of vibrating diatomic molecules. These turning points are then used to construct the potential energy curve and, thereby, garner the wavefunctions needed to calculate the transition probabilities. RKR does not rely on the actual spectral data nor the energy eigenvalues for this operation, but molecular constants.

Problems can arise from reducing large sets of spectroscopic data into molecular constants. "Because of the inadequacy of the Born-Oppenheimer separation of the total molecular energy into electronic, vibrational, and rotational parts, a large number of molecular constants must be introduced to account for the energy level structure of the molecule. These constants appear in the expressions for the levels in an often complex and nonlinear manner so that their determination poses a burdensome problem ... Moreover, additional difficulties may arise from the need to determine the molecular constants using proper statistics." (6:38) With these difficulties in mind, and possible

systematic errors in the rotational constants “within the experimental limit (are) sufficient to cause substantial non-physical behavior in the potential obtained on inversion.” (7:248)

This non-physical behavior often manifests itself in the repulsive branch of the potential. The repulsive arm can either have a ripple or may bend over (7:244) making the potential double-valued and non-physical, typically at the higher energy levels which have greater experimental uncertainty or are unknown. This situation leaves the transition calculations for the higher energy levels suspect. Tellinghuisen and Henderson (8) circumvent this problem by replacing the repulsive branch of the potential with the Morse potential (9). However, this technique does not attack nor change the fundamental problem of with the RKR-IPA method, that being this method sometimes yields pathological potential energy curves.

In 1984, Shankland, Dorko, and Ostdiek developed a new approach to find the potential energy curve for diatomic molecules (10). Their method, unlike RKR, is a quantum mechanical approach, and uses the actual absorption and emission spectral data for its calculations. This numerical technique, involves a finite element solution of Schrödinger's Equation for a given potential energy curve. Each computed eigenvalue, along with its associated experimental eigenvalue, is then compared and a residual is recorded. The potential energy function is constructed so that a non-linear minimization routine can then vary the parameters within this function. Then for each new potential curve selected by the minimization routine, Schrödinger's Equation is re-solved. Thereby, through an iterative process, the potential curve which yields the smallest residual is found. The wave functions can now be garnered from this potential. Along with the

wave functions from another electronic state, the transition probabilities are then calculated.

The Shankland-Dorko-Ostdiek (SDO) method has several advantages over the RKR method. One, it is completely a quantum mechanical approach, not a hybrid of classical and quantum mechanics. Therefore, its solutions are rooted in physical law and theory as understood today. Second, it bypasses the problems RKR encounters with molecular constants by using eigenvalues derived directly from the spectroscopic data. This spectroscopic data does not have to be reduced into spectroscopic constants, but only assigned to the proper transition. Lastly, any potential function can be used for the fit. Possibilities include the Morse, Lennard-Jones, Mie potentials, or even a custom potential function. Therefore, this method will never render a potential function which is pathological. The accumulative effect of these advantages means that this method has the prospect of yielding results of greater accuracy than RKR, especially at the higher energy states.

However, the SDO method, after initial development, underwent very little testing and evaluation. Many questions went left unanswered. Will this numerical technique converge for sophisticated potentials such as a Morse or a Mie? Will this method work for a real molecule?

Objectives

The main objective of this research is to validate the SDO method as a reliable numerical solution of Schrödinger's Equation. Reliability and accuracy will be determined by comparing the numerical eigenvalues and functions with the analytical solutions of oscillators such as the Harmonic and Morse. Second, demonstrate that this method can be used for finding the potential energy curve of a molecule which is previously known.

Scope

The scope of this research project is to validate the use of this numerical technique to predict energy transitions and their associated probabilities for diatomic molecules. Validation will include comparisons to the analytical solutions of a simple harmonic, analytical solutions of an anharmonic oscillator, and one real molecule with a large, accurate, empirical knowledge base. This study is only concerned with the analysis of diatomic molecules, even though this code with some modification could be extended to linear triatomics or even more complicated molecules. No attempt will be made to collect any spectroscopic data in a laboratory environment, only published spectroscopic data will be used. Also, no effort will be made to apply this code to predict undiscovered data for some arbitrary molecule.

Approach

This thesis report is organized in a linear fashion starting with theory and background, and ending with validation studies. The objective of this organization is convince the reader that this numerical approach is a reliable tool for calculating transition probabilities for diatomic molecules.

Chapter II begins to lay the theoretical foundation by relating Einstein's Coefficients to the Franck-Condon Factors through a quantum mechanical treatment. This development is followed by a discussion of molecular forces, and the electronic shepherding which is this binding force. These molecular forces can be approximated by the Harmonic and Morse Oscillators. The analytical solutions of these potentials are shown in prelude to a discussion about the Franck-Condon Principle. Unfortunately, real molecules do not behave like these potentials, which leads to the requirement for numerical techniques such as the SDO method. The rest of the chapter is dedicated to this method of finite elements as used to solve Schrödinger's Equation.

Chapter III continues with this thought by explaining how the SDO method is implemented on a computer. Discussions include how spectroscopic data is converted into a format acceptable to the model, how the model searches and finds the "best" potential surface with a non-linear minimization routine, and how the Franck-Condon

Factors are calculated using the eigenfunctions garnered from this optimal surface. These discussions include a basic recipe for executing each section of the code.

Finally, chapter IV demonstrates that this numerical technique is a valid approach for solving Schrödinger's Equation. This validation is accomplished by comparing the analytical and numerical solutions of the Harmonic and Morse Oscillators. Then, a known potential surface for the hydrogen molecule is used as a test to see if indeed this potential surface could find this potential in the blind.

A concluding chapter summarizes these results and presents recommendations for more research.

II . Literature Background and Theory

Introduction

The motivating force behind this research is to develop a tool a laser engineer can use to analyze the electronic and vibrational transitions taking place within the gain medium. In order to analyze these transitions, the quantum mechanical or molecular properties of this gain medium must be known.

Therefore, this chapter introduces the theory and concepts needed to understand how the Shankland-Dorko-Ostdiek (SDO) numerical technique reveals these quantum mechanical properties of the molecule. First, an overview of transition theory lays the foundation for what knowledge is required of the molecule for the laser engineering analysis to happen, namely the Franck-Condon Factors related through Einstein's Coefficients. To calculate these factors, quantum mechanics is invoked to garner the molecule's wave functions. Therefore, a short discussion follows which sets up Schrödinger's Equation, a solution of which gives the wave functions, and shows how several different potential functions can be used to approximate the molecular forces. The SDO technique, a solution for Schrödinger's Equation numerically using a finite element method, is briefly explained. Finally, with the wave functions in hand, the last section outlines the procedure for using the wavefunctions to calculate the Franck-Condon Factors, and describes the principle on which they are founded.

Laser Transitions

A laser (Light Amplification by Stimulated Emission of Radiation) is a device which utilizes the natural energy transitions of atoms and molecules to produce a coherent, amplified, and monochromatic source of electromagnetic radiation. For an in-depth discussion of lasers see Verdeyen (1).

Briefly, however, a fundamental requirement to initiate lasing is to establish a population inversion between two transition levels. This non-equilibrium state is accomplished by pumping the molecules of the gain medium from a lower energy state to an upper state with an external energy source. These excited molecules then relax back to their ground state, giving up their energy through either radiative or non-radiative events. The wavelength of the radiation is determined by the difference in energy between the two states on which the transition happened. The rate of the radiative processes described by the Einstein Coefficients, coupled with the non-radiative rates determine if the population inversion can be sustained. If the population inversion is lost, the lasing activity ceases. Figure II-1 illustrates the transition process for a hypothetical four level laser.

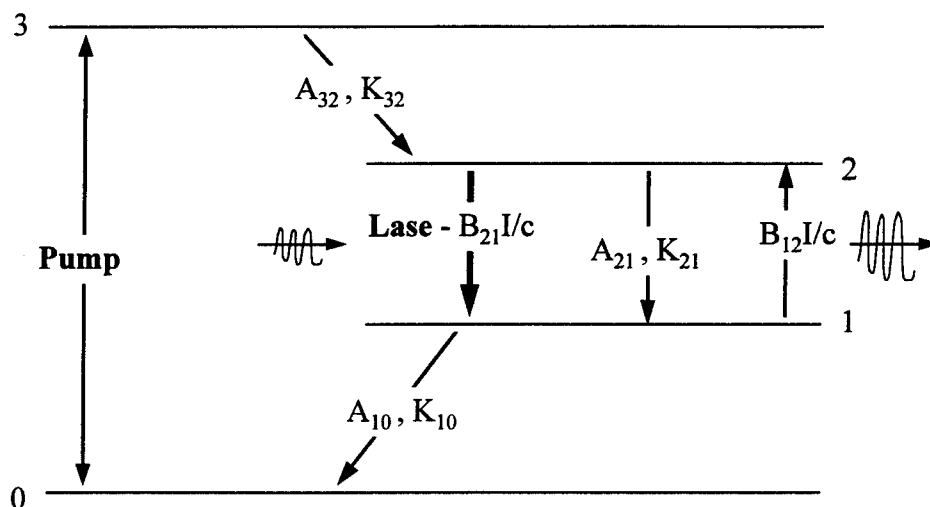


Figure II-1 This schematic diagram shows a possible arrangement of the energy levels for the gain medium of a laser. The pumping action promotes some of the ground state's population (labeled 0) to the highest energy level. From this energy level, the excited population relaxes back to the ground via the path and rates as indicated. Note: the rates are also proportional to the population of the states initiating the transition. Lasing actually occurs on the transition from state 2 to 1, where the field stimulates emission adding constructively more energy to the field. Einstein's Coefficients are labeled A and B (for a more detailed definition see the following discussion), the rate of non-radiative processes are indicated by the symbol K, I is the intensity of the lasing field, and c is the speed of light.

The determination of these process rates called Einstein's Coefficients, therefore, are critical to the transition analysis of any laser. These coefficients can be derived through time-dependent perturbation theory of Schrödinger's Equation (2:TP1-TP12b; 3:267-277; 6:12-18,24-25). If the Hamiltonian, a quantum mechanical representation of the atom's or molecule's energy, is perturbed by an in-coming time-dependent electromagnetic field then the rate of transition, or absorption for this example, is found to be

$$R_{k \rightarrow m} = \frac{4\pi^3}{3ch^2\epsilon_0} I(\omega_{mk}) \left| \langle m | \mu | k \rangle \right|^2 \quad (\text{II-1})$$

where R is the rate of transition from state k to state m, k is the initial state of the system, m is the final state, c is the speed of light, h is Planck's constant*, ϵ_0 is the permittivity of free space, I is the intensity of the electromagnetic field at the frequency ω_{mk} corresponding to the transition, μ is the electric dipole operator, and $\left| \langle m | \mu | k \rangle \right|^2$ is defined as the transition moment.

In Figure II-1, for example, k would be state 1 and m would be state 2. Therefore, the absorption rate from energy state 1 to 2, indicated by $B_{12} I/c$, must be the same quantity as defined by Equation II-1. With that, setting them equal to each other and keeping the units straight yields

$$B_{mk}^{abs} = \frac{4\pi^3}{3h^2\epsilon_0} \left| \langle m | \mu | k \rangle \right|^2 \quad (\text{II-2})$$

Now if the pump was turned off, and the system allowed to reach thermal equilibrium, the relationship governing the populations of states 2 and 1 must still hold at thermodynamic equilibrium. Each radiative process going down in energy must equal

* Special note: due to a font limitation, hbar will always be written as $h/2\pi$. Also, the 2π factor may be simplified into the expression.

each process going up. Therefore, the time rate of change of each population for level 1 and 2 must be equal to each other. Mathematically this means

$$\left. \frac{dN_2}{dt} \right|_{\text{radiative}} = -A_{21}N_2 + B_{12}N_1\rho(\omega_{21}) - B_{21}N_2\rho(\omega_{21}) = -\left. \frac{dN_1}{dt} \right|_{\text{radiative}} = 0 \quad (\text{II-3})$$

must be true. Where $N_{1,2}$ is the population of each respective level, $\rho(\omega_{21})$ is the energy density of the field previously referred to as $I(\omega_{mk})/c$, A_{21} is the probability per second for spontaneous emission of a photon, $B_{12} \rho(\omega_{21})$ is the probability per second for absorption of a photon, and $B_{21} \rho(\omega_{21})$ is the probability per second of spontaneously emitting a photon. Since, the system is at thermal equilibrium, $\rho(\omega_{21})$ must be equal to energy density defined by Planck's Blackbody formula. This formula is

$$\rho(\nu_{21}) = \frac{8\pi h \nu_{21}^3}{c^3} \left[e^{\frac{h\nu_{21}}{kT}} - 1 \right]^{-1} \quad (\text{II-4})$$

where ν_{21} is the frequency of light equal to $\omega_{21}/2\pi$, k is Boltzman's constant, and T is the temperature at thermal equilibrium (6: 24).

Solving Equation II-3 for $\rho(\omega_{21})$ and setting it equal to Planck's Blackbody formula, "Einstein forced the fit with identification of various interrelationships between

the coefficients" (4:182). Designating the degeneracy of each respective level as $g_{1,2}$, Einstein found

$$g_2 B_{21} = g_1 B_{12} \quad (\text{II-5})$$

$$A_{21} = \frac{h \omega_{21}^3}{2\pi^3 c^3} B_{21} = \frac{h \omega_{21}^3}{2\pi^3 c^3} \frac{g_1}{g_2} B_{12}$$

Casting in general terms, Einstein's Coefficients become

$$\begin{aligned} B_{k \rightarrow m}^{\text{abs}} &= \frac{g_m}{g_k} B_{mk} = \frac{4\pi^3}{3h^2 \epsilon_0} \left| \langle m | \mu | k \rangle \right|^2 \\ A_{m \rightarrow k} &= \frac{h \omega_{mk}^3}{2\pi^3 c^3} B_{mk} = \frac{g_k}{g_m} \frac{2\omega_{mk}^3}{3c^3 \epsilon_0} \left| \langle m | \mu | k \rangle \right|^2 \end{aligned} \quad (\text{II-6})$$

The transition moment can be further simplified for the simple case of diatomic molecules. Using the Born-Oppenheimer (5) approximation, the wavefunction for each state, m and k , can be separated into independent electronic, vibrational, and rotational functions. Therefore, the total diatomic wavefunction for each state can be expressed as (6:136-137)

$$\begin{aligned} |m\rangle &= |\Psi_{el}^m\rangle |X_v^m X_J^m\rangle \\ |k\rangle &= |\Psi_{el}^k\rangle |X_v^k X_J^k\rangle \end{aligned} \quad (\text{II-7})$$

where Ψ_{el} represents the electronic wave function, X_v represents the vibrational wave function of the molecule, X_J represents the rotational wavefunction of the molecule, and \mathbf{r} and \mathbf{R} represent the sets of electronic and nuclear coordinates, respectively.

Since changes in electronic, vibrational, and rotational states are possible both \mathbf{r} and \mathbf{R} dependencies must be considered in the dipole operator μ when calculating electric dipole (E1) transition probabilities. Therefore, the dipole operator may be written as

$$\mu = - \sum_i e \mathbf{r}_i + \sum_N e Z_N \mathbf{R}_N \equiv \mu_{el} + \mu_{nucl} \quad (\text{II-8})$$

Where e is the charge of an electron, i is an index for each electron in the molecule, Z is the charge of the nucleus, and N is the index for each nuclei.

Ignoring the rotational behavior of the molecule (for simplicity) the transition moment becomes

$$\begin{aligned} \langle m | \mu | k \rangle &= \langle \Psi_{el}^m X_v^m | \mu_{el} + \mu_{nucl} | \Psi_{el}^k X_v^k \rangle \\ &= \langle \Psi_{el}^m | \mu_{el} | \Psi_{el}^k \rangle \langle X_v^m | X_v^k \rangle + \langle \Psi_{el}^m | \Psi_{el}^k \rangle \langle X_v^m | \mu_{nucl} | X_v^k \rangle \\ &= M_e(\mathbf{R}) \langle X_v^m | X_v^k \rangle + 0 \end{aligned} \quad (\text{II-9})$$

Each dipole operator only operates on its corresponding wavefunction. Therefore, each dipole operator is distributed, and after some factoring, each then operate on its corresponding wavefunction. The following simplifications are then made. Immediately,

the second term goes to zero because the two electronic wavefunctions are orthogonal to each other. The first term, however, does not go to zero because the two vibrational wavefunctions are from two distinct basis sets and not necessarily orthogonal. The integration of $\langle \Psi_{el}^m | \mu_{el} | \Psi_{el}^k \rangle$ over \mathbf{r} yields the transition moment, $M_e(\mathbf{R})$. $M_e(\mathbf{R})$ is a function of nuclear position \mathbf{R} because the electronic wave functions depend on both \mathbf{r} and \mathbf{R} . However, if $M_e(\mathbf{R})$ is assumed to vary slowly with \mathbf{R} , then further simplification yields

$$\begin{aligned} \langle m | \mu | k \rangle &= \overline{M_e(R)} \langle X_v^m | X_v^k \rangle \\ &= \overline{M_e(R)} \langle v' | v'' \rangle \end{aligned} \tag{II-10}$$

where $\overline{M_e(R)}$ is the average value of the electronic transition moment. From here on, a shorthand is introduced to represent the upper electronic state's vibrational wavefunction as v' , and v'' will represent the lower electronic state's vibrational wavefunction. The probability of the electronic transition is then proportional to the total transition moment squared, or in mathematical terms $|\langle m | \mu | k \rangle|^2$. Then, substituting Equation II-10 into Equation II-6 produces the final result

$$\begin{aligned}
 B_{k \rightarrow m}^{\text{abs}} &= \frac{g_m}{g_k} B_{mk} = \frac{4\pi^3}{3h^2 \epsilon_0} \overline{M_e(R)^2} \left| \langle v' | v'' \rangle \right|^2 \\
 A_{m \rightarrow k} &= \frac{h\omega_{mk}^3}{2\pi^3 c^3} B_{mk} = \frac{g_k}{g_m} \frac{2\omega_{mk}^3}{3c^3 \epsilon_0} \overline{M_e(R)^2} \left| \langle v' | v'' \rangle \right|^2
 \end{aligned}
 \tag{II-11}$$

where $\left| \langle v' | v'' \rangle \right|^2$ is defined as the Franck-Condon Factor. The Franck-Condon Principle is discussed in detail later. Thus, Einstein's Coefficients are directly proportional to the Franck-Condon Factors for diatomic molecules.

Diatomic Molecules

Clearly, the Franck-Condon Factors are important to laser engineering in regards to transition analysis. To calculate these factors, Schrödinger's Equation must be solved for the molecule of interest. The following discussion outlines the theory and procedure for solving Schrödinger's Equation analytically.

For simplicity, imagine a reduced mass representation of a vibrating molecule that is fixed in space, i.e. not translating, and not rotating. Then Schrödinger's Equation may be expressed as (7:98-101)

$$(\tilde{H} - E) \Psi_{\text{vib}} = -\frac{h^2}{8\pi^2 \mu} \frac{\partial^2 \Psi_{\text{vib}}}{\partial R^2} + [V(R) - E_{\text{vib}}] \Psi_{\text{vib}} = 0
 \tag{II-12}$$

where \tilde{H} is the Hamiltonian Operator, E is the energy of molecule, Ψ_{vib} is the wavefunction which describes the nuclear position, μ is the reduced mass of the molecule, R is the internuclear separation, and $V(R)$ is the potential energy of the system as a function of R . If the potential, $V(R)$, is known, then Equation II-12 written in matrix form can be diagonalized, thereby, garnering the wavefunctions and energies and ultimately the Franck-Condon Factors are calculated from the wavefunctions.

Physically, $V(R)$ represents the force, related by $F_{A \leftrightarrow B} = -\frac{\partial V(R)}{\partial R}$, which binds

the two atoms together into one molecule. This force arises from the variation of total electronic energy with internuclear separation. In other words, the molecular electron cloud shepherds the two nuclei keeping them bundled together. This shepherding process overcomes the nuclear-nuclear repulsive forces yearning to dissociate the molecule.

This shepherding process is extremely complex. In principle, however, the complete Hamiltonian could be written down for the entire molecular system. This expression would include all of the forces, such as the Coulombic electron-nuclear attractive and electron-electron repulsive forces, the rotational terms, spin coupling, relativistic corrections, and so on. But these Hamiltonians are extremely difficult to solve, even for the simplest of molecules like H_2 . Therefore, one way to avoid this problem is to lump all of these terms together, call it $V(R)$, and, thereby, analyze only the accumulative molecular potential.

This potential energy surface, however, cannot be represented by any one general function for all diatomic molecules. There are, however, some general properties the

potential must possess to model the physical behavior correctly. One, it must be smooth and continuous. This condition ensures the force is always finite. Second, the function needs to be always single valued. That is, at any given internuclear separation, only one energy configuration is allowed. Next, as internuclear distance goes to infinity the molecular forces must go to zero to allow for dissociation, therefore, the slope of the potential must go to zero. Conversely, as the internuclear distance approaches zero the nuclear-nuclear repulsive forces increase dramatically. Therefore, the slope of the potential needs to be steep and negative to model this force. Finally, a stable molecule implies an equilibrium position exists where the force is zero, i.e. the potential energy is at a minimum. Figure II-2 illustrates such potential energy surface.

Intermolecular Force Model

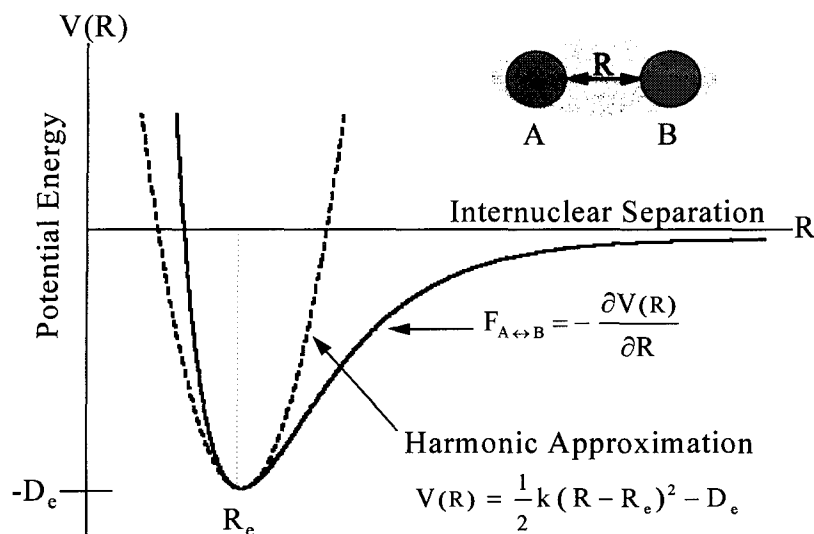


Figure II-2. This figure illustrates the intermolecular force model. The potential energy curve, $V(R)$, drawn with the solid line exemplifies all of the characteristics needed to model the intermolecular forces, $F_{A \leftrightarrow B}$, between atoms A and B. The steep repulsive branch captures the large forces the two nuclei experience at small R , and the attractive branch on the right allows the molecule to dissociate at large internuclear separations. The well defines the region of a lower energy configuration centered by the radius of equilibrium, R_e , where the energy is a minimum. D_e is dissociation energy as defined from the bottom of the well to the dissociation limit. The graph of the harmonic oscillator shows where this approximation is valid.

A Taylor expansion of some general potential, $V(R)$, which meets these conditions, about the equilibrium position, R_e , yields

$$\begin{aligned}
 V(R) &= V(R) \Big|_{R=R_e} + (R - R_e) \left(\frac{\partial V(R)}{\partial R} \right) \Big|_{R=R_e} + \frac{1}{2!} (R - R_e)^2 \left(\frac{\partial^2 V(R)}{\partial R^2} \right) \Big|_{R=R_e} + \dots \\
 &\approx -D_e + 0 + \frac{1}{2} k (R - R_e)^2
 \end{aligned}
 \tag{II-13}$$

where the value of the potential at R_e is $-D_e$ (the dissociation energy). The first derivative vanishes at R_e because the potential is at a minimum. A constant, k , is the curvature of the potential. Figure II-2 illustrates this Taylor expansion as the dashed curve. This truncated expansion is immediately recognized as the harmonic oscillator.

The solution of Schrödinger's Equation for the harmonic oscillator is (8:176-202)

$$\begin{aligned} E_n &= \frac{h \omega}{2\pi} \left(n + \frac{1}{2} \right) \quad n = 0, 1, 2, \dots \\ \Psi_n &= \left(\frac{\sqrt{\alpha}}{2^n n! \sqrt{\pi}} \right) e^{-q^2/2} H_n(q) \end{aligned} \quad (\text{II-14})$$

Where E_n is the energy of state n , ω is the angular frequency of the oscillation equal to

$\sqrt{\frac{k}{\mu}}$, k is the force spring constant, μ is the reduced mass, Ψ_n is the eigenfunction of

state n , $\alpha = \omega \mu \left(\frac{2\pi}{h} \right)$, $q = \sqrt{\alpha} x$, $x = (R - R_e)$, and $H_n(q)$ is the Hermite polynomial

$(-1)^n e^{q^2} \frac{\partial^n}{\partial q^n} e^{-q^2}$. Figure II-3 shows 4 wave functions for this simple oscillator.

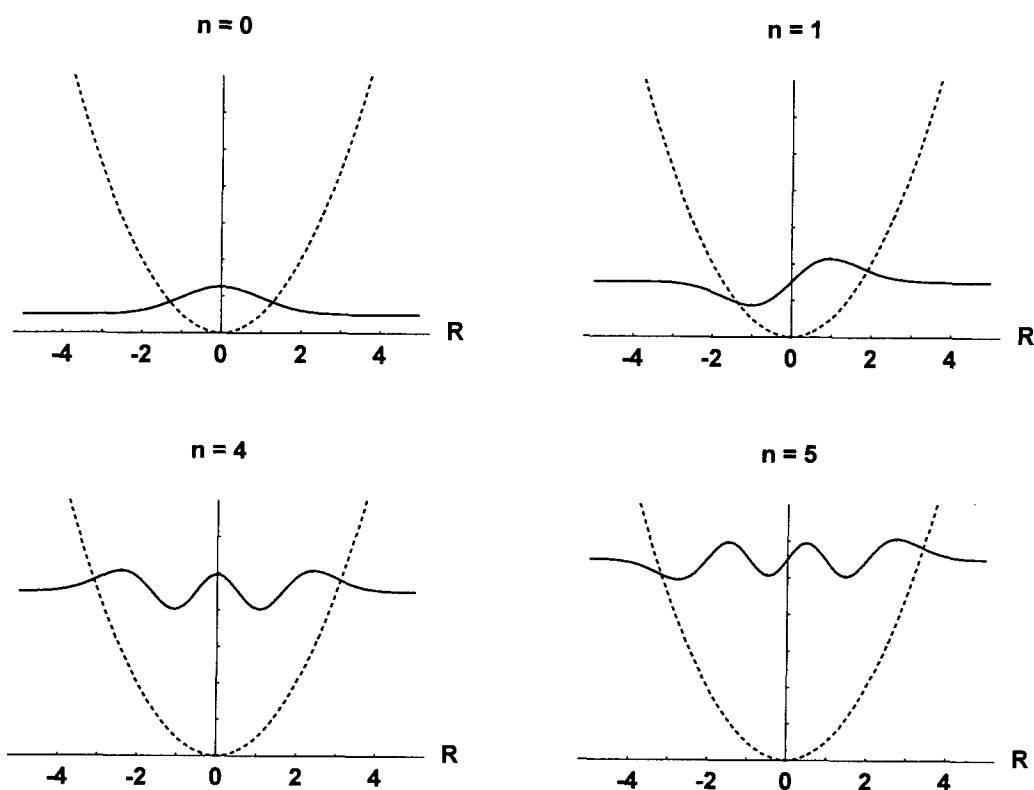


Figure II-3. This graphic shows four eigenstates of the harmonic oscillator (9:67-73). Each eigenfunction is plotted at its corresponding energy level for illustrative purposes only, the amplitude of the waves have units of $\text{probability}/(\text{unit length})^{1/2}$. Notice each wavefunction is symmetric about the radius of equilibrium, R_e , and the number of nodes corresponds to its state number. The amplitude squared of these wavefunctions is the probability of finding the reduced mass particle at that location. Notice, the wavefunctions imply the particle can actually tunnel through its classical turning point, where the wavefunctions crosses the potential curve. Plotted with Mathematica®.

The utility of this harmonic approximation is limited to the region very near equilibrium. Morse proposed instead the following function as a suitable approximation for the diatomic molecular energy curve (10)

$$V(r) = D_e e^{-2a(R-R_e)} - 2D_e e^{-a(R-R_e)} \quad (\text{II-15})$$

where a is referred to as the anharmonicity term. This variable has units of inverse length. See Figure II-4 for an illustration of the Morse potential.

The width of the Morse potential at half max, $\Delta W_{1/2}$, is inversely proportional to a . Therefore, the larger a is, the stronger the molecular forces are, and the narrower the well becomes. The dissociation energy D_e stretches the well vertically. D_e and a determine the number of bound states which are allowed by this potential. Large D_e and small a yield large numbers of bound states.

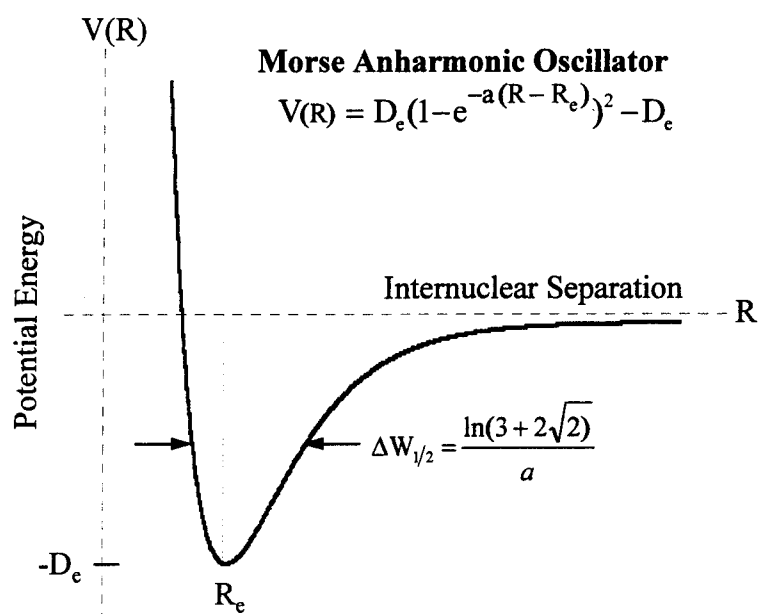


Figure II-4. This figure illustrates the Morse Potential. This curve exhibits all of the characteristics required to model molecular forces. In fact, this model is a good approximation, however, no molecule is known to exactly mimic the Morse Oscillator. The width at half max, $\Delta W_{1/2}$, is inversely proportional to a . Therefore, the larger a is, the stronger the molecular forces are, and the narrower the well becomes. The dissociation energy parameter D_e stretches the well vertically.

Morse analytically calculated the eigenvalues and functions for this oscillator as

$$E_n = -D_e + \frac{\hbar\omega}{2\pi} \left(n + \frac{1}{2} \right) - \frac{\hbar^2\omega^2}{16\pi^2 D_e} \left(n + \frac{1}{2} \right)^2 \quad n = 0, 1, 2, 3, \dots$$

$$\Psi_n = \sqrt{\frac{2da}{N^2}} e^{\frac{-z}{2}} z^{\frac{b}{2}} L_n^b[z]$$

(II-16)

where n is a non-negative integer which labels the eigenstate, $\omega = a \sqrt{\frac{2D_e}{\mu}}$,

$$d = \frac{2\pi\sqrt{2\mu D_e}}{ha}, N^2 = \frac{(n+b)!}{n!}, b = k-1-2n, k=2d, z = 2d e^{-a(R-R_e)}, \text{ and } L_n^b[z] \text{ is the}$$

Associated Laguerre Polynomial (11: 59-60; 12: 725-726) given by

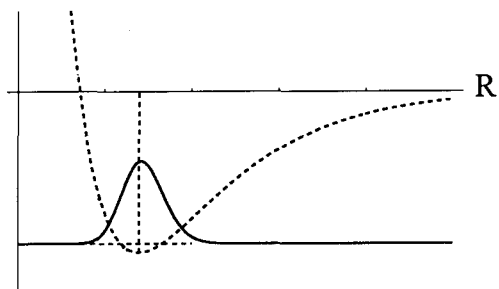
$$L_n^b[z] = \sum_{m=0}^n (-1)^m \frac{(n+b)!}{(n-m)!(b+m)!m!} z^m, \quad b > -1 \quad (\text{II-17})$$

Morse commented that this was the first solution of Schrödinger's Equation which yielded a finite number of discrete energy states. In fact, the condition on b (see Equation II-17) for the Laguerre Polynomial to be defined implies n must always be less than d .

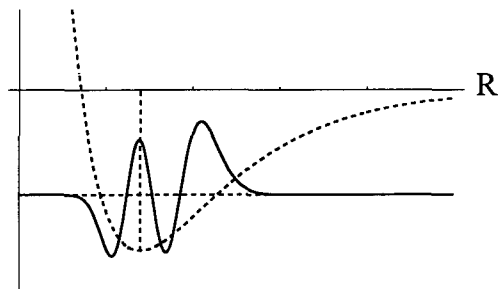
Expressed mathematically this condition is

$$n \leq \frac{2\pi\sqrt{2\mu D_e}}{ah} \quad \text{where } n = 0, 1, 2, 3, \dots \quad (\text{II-18})$$

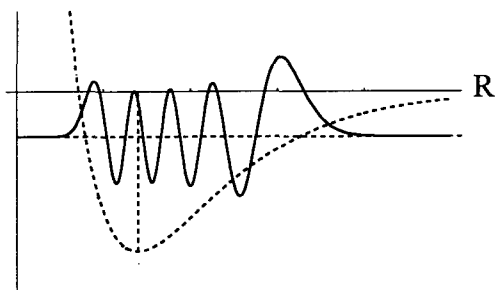
$n = 0$



$n = 3$



$n = 8$



$n = 11$

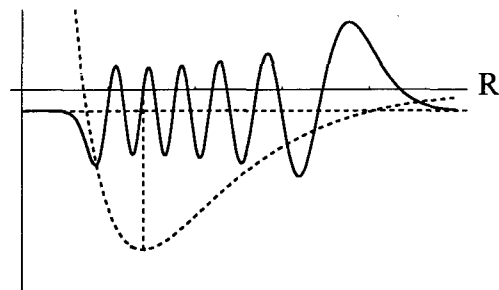


Figure II-5. This figure illustrates 4 eigenfunctions of a Morse Oscillator. Each eigenfunction is plotted at its corresponding energy level for illustrative purposes only, the amplitude of the waves have units of $\text{probability}/(\text{unit length})^{1/2}$. Notice each wavefunction is asymmetric about the radius of equilibrium, R_e . R_e is denoted by the dashed vertical line. The wavefunctions are stretched towards the classical turning point associated with the attractive branch. The large amplitudes imply the probability of finding the reduced mass particle at this location is greatest here. Notice the ground state ($n=0$) is very similar to the Harmonic Oscillator's (see Figure II-3). This region of the well can be approximated by a harmonic oscillator. Plotted with Mathematica®.

Circling back, the Morse Oscillator can itself be approximated by the Harmonic Oscillator near equilibrium. The force constant k of the Harmonic Oscillator can be related to the Morse Oscillator by expanding it into a Taylor Series(see Equation II-13). This relationship is found by setting the second order term of the expansion equal to the Harmonic Oscillator yielding

$$k = 2 D_e a^2 \quad (\text{II-19})$$

Franck-Condon Principle

“The Franck-Condon Principle governs the intensity of spectral transitions between the vibrational levels of different electronic states of molecules.”(13:78-81). Therefore, as discussed earlier, the Franck-Condon Principle is central to the process of determining laser line transition probabilities. The following section describes the Franck-Condon Principle in more detail.

By recognizing the great difference between the masses of the electrons and nuclei, the Born-Oppenheimer approximation can be invoked. Consider two different molecular states, then each state can be separated into electronic, vibrational, and rotational wavefunctions. Recalling Equation II-7, the wavefunction were separated and written as

$$|m\rangle = |\Psi_{el}^m\rangle |X_v^m X_J^m\rangle \quad (II-20)$$

$$|k\rangle = |\Psi_{el}^k\rangle |X_v^k X_J^k\rangle$$

Then Equation II-9 allows us to calculate the E1 transition between these states as (ignoring rotation)

$$\begin{aligned} \langle m | \mu | k \rangle &= \overline{M_e(R)} \langle X_v^m | X_v^k \rangle \\ &= \overline{M_e(R)} \langle v' | v'' \rangle \end{aligned} \quad (II-21)$$

where $\overline{M_e(R)}$ is the average electronic transition moment, and $\langle v' | v'' \rangle$ is defined as the vibrational overlap integral. The double prime notation traditionally represents the lower electronic state, and single prime the upper state. The electronic transition moment, a resultant of the two electronic wavefunctions and the dipole operator, is averaged over the range of R and is considered constant. The probability of making a transition from v' to v'' is then given by the absolute value of Equation II-21 squared where the Franck-Condon Factor is defined as the quantity

$$q_{v'v''} = \left| \langle v' | v'' \rangle \right|^2, \text{ where } 0 \leq q_{v'v''} \leq 1 \quad (II-22)$$

where v' and v'' are two vibrational wavefunctions each from a different electronic state. For illustrative purposes, Figure II-6 shows several Morse wavefunctions depicting

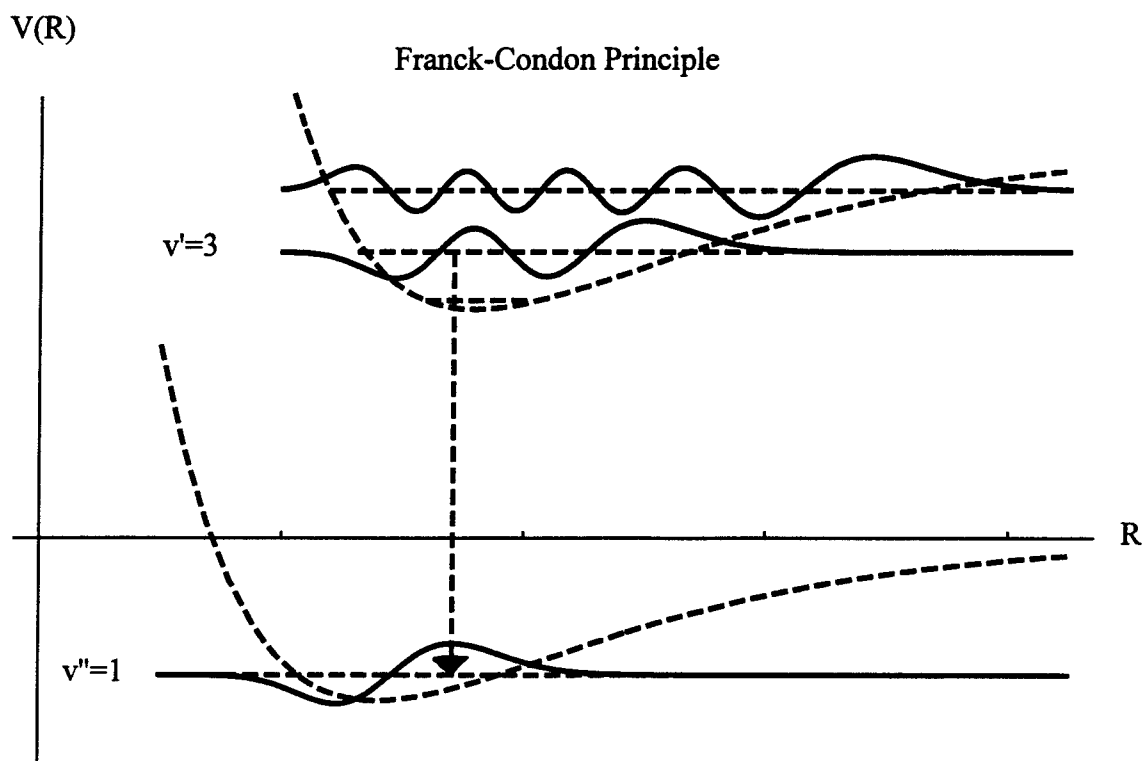


Figure II-6. This figure illustrates the concept of the Franck-Condon principle. Transitions occur vertically where the overlap integral is non-zero. Following the Born-Oppenheimer approximation, the electronic transition happens so fast that the nuclei can be considered to be at rest. In other words, from the start of the transition to the end of the transition, the nuclei will not have moved. Therefore, a transition can only occur from one state to the next if the nuclei have a probability of existing at that location in both states.

the vibrational states v' and v'' . These vibronic (a contraction of the words vibrational and electronic) transitions seldom occur without a change in the vibrational state label. For example, the upper electronic state might be at vibrational level 3 and then transition down to the lower electronic state with a vibrational state of 1 as depicted in Figure II-6.

These transitions are considered to be vertical. That is, the transitions take place at a fixed nuclear separation. The Born-Oppenheimer approximation, based on the large differences between the masses of the electrons and nuclei, establishes also that the relative kinetic energy of the electrons is extremely large compared to the nuclei. Therefore, during a vibronic transition the electronic molecular cloud reconfigures itself so quickly that the nuclei virtually haven't moved in this time frame. With the nuclei being fixed in position, the probability of this vibronic transition can only be non-zero if and only if the nuclei have a probability of existing at this location in both states.

Summing all of the Franck-Condon Factors from one vibrational state in the upper electronic state to all of the vibrational states of the lower electronic state

$$\begin{aligned}
 \sum_{v''} q_{v'v''} &= \sum_{v''} \left| \langle v' | v'' \rangle \right|^2 \\
 &= \sum_{v''} \langle v' | v'' \rangle \langle v'' | v' \rangle, \text{ but } \sum_{v''} |v'' \rangle \langle v''| = 1 \\
 \therefore \sum_{v''} q_{v'v''} &= \langle v' | v' \rangle = 1
 \end{aligned} \tag{II-23}$$

where closure has been invoked to eliminate the summation. Since v' is orthogonal with itself, the expression reduces to 1. Or simply put, a single vibrational state in the upper

electronic level has a 100% probability of transitioning to some vibrational level in the lower electronic state.

Certainly then, if the vibrational wavefunctions are known for each electronic state, each and every Franck-Condon Factor can be calculated.

Numerical Solution of Schrödinger's Equation

Numerical methods are essential for any realistic molecular potential functions. The Harmonic and Morse potentials are functions which can be reduced analytically. Unfortunately, nature does not provide molecular potential curves which behave so nicely as these. Real molecular potential functions can't be modeled by simple functions due to the sophistication and complexity of the electronic molecular cloud. This complexity means an analytic solution for the vibronic wavefunction may never be found for molecules.

Previous to 1984, the Air Force Institute of Technology used the customary tool, the RKR-IPA method, to numerically calculate the Franck-Condon Factors of diatomic molecules. Even with fine tuning and "work arounds", the RKR method was limited to the lowest vibrational states (See Chapter I, The Introduction). Therefore, Shankland, Dorko, and Ostdiek sought to develop a new and better method. The technique they developed, which exploits the method of finite elements, abandoned all of the methods

previously employed by the spectroscopy community. Even though this method of finite elements was new to this community, it was certainly not to the engineering world.

The emergence of computers was the genesis of the finite element method. Computers enabled scientists and engineers to tackle problems previously unsolvable. Mathematical techniques such as the classical Rayleigh-Ritz method, variational calculus, and Galerkin's weighted residuals method, much developed at the turn of the century, were assembled into what's now called the finite element method. This method was first developed in the early 1950's "to solve continuum problems in elasticity using small discrete elements to describe the overall behavior of simple elastic bars..." (14:1-2) Over time, this method grew in sophistication and has been used successfully to analyze an eclectic assortment of problems, such as electromagnetism, heat conduction, fluid flow, and mechanical stresses, even in three dimensions.

The SDO method finds the "best" empirical molecular potential in an exhaustive search. Central to this search algorithm is a numerical solution of Schrödinger's Equation solved with the method of finite elements. The following discussion explains briefly how the finite elements method is used to solve Schrödinger's Equation. Later, the Computer Modeling Chapter explains how this technique is used in an iterative fashion to find the best potential.

Schrödinger's Equation in the coordinate representation is

$$(\tilde{H} - E) \Psi_{\text{vib}} = -\frac{\hbar^2}{8\pi^2\mu} \nabla^2 \Psi_{\text{vib}} + [V(R) - E_{\text{vib}}] \Psi_{\text{vib}} = 0 \quad (\text{II-24})$$

where $V(R)$ captures only the vibrational energies. For simplicity the rotational energies are ignored. This simplification means that this algorithm will not handle rotational energies. Rewriting Equation II-24 in the time independent Dirac notation yields

$$\begin{aligned}
 \tilde{\mathbf{H}} \left| \Psi_{\text{vib}} \right\rangle &= E \left| \Psi_{\text{vib}} \right\rangle \\
 \langle \Psi_{\text{vib}} | \tilde{\mathbf{H}} | \Psi_{\text{vib}} \rangle &= E \langle \Psi_{\text{vib}} | \Psi_{\text{vib}} \rangle \\
 \therefore E &= \frac{\langle \Psi_{\text{vib}} | \tilde{\mathbf{H}} | \Psi_{\text{vib}} \rangle}{\langle \Psi_{\text{vib}} | \Psi_{\text{vib}} \rangle} = \frac{\langle \Psi_{\text{vib}} | \frac{\tilde{\mathbf{P}}^2}{2\mu} + V(R) | \Psi_{\text{vib}} \rangle}{\langle \Psi_{\text{vib}} | \Psi_{\text{vib}} \rangle}
 \end{aligned} \tag{II-25}$$

The wavefunction is assumed to be spherically symmetric, therefore, in the coordinate representation $\frac{\tilde{\mathbf{P}}^2}{2\mu} \rightarrow -\frac{\hbar^2}{8\pi^2\mu} \frac{1}{R^2} \frac{\partial}{\partial R} R^2 \frac{\partial}{\partial R}$ and integration is conducted over the volume element $\partial\tau = 4\pi R^2 \partial R$. With the substitution of $\Psi_{\text{vib}} = \frac{U(R)}{R}$, Ostdiek showed (15:18-36), with the aid of integration of parts, that Equation II-25 can be cast in the weak form in the coordinate representation as

$$E = \frac{\frac{\hbar^2}{8\pi^2\mu} \int_0^\infty \left(\frac{\partial U(R)}{\partial R} \right)^2 \partial R + \int_0^\infty U^2(R) V(R) \partial R}{\int_0^\infty U^2(R) \partial R} \tag{II-26}$$

where now $\partial\tau = \partial R$. U is now treated as the spherical wavefunction.

To employ the finite element method, a grid is laid over the space of integration. The goal of finite elements is to approximate the integral (the value of the function) in each discretized element. Since this problem has been reduced to one dimension, each element has the step length of h (not to be confused with Planck's constant). Each local element is then transformed by a natural coordinate system to ease integration later.

Figure II-7 illustrates the finite element grid.

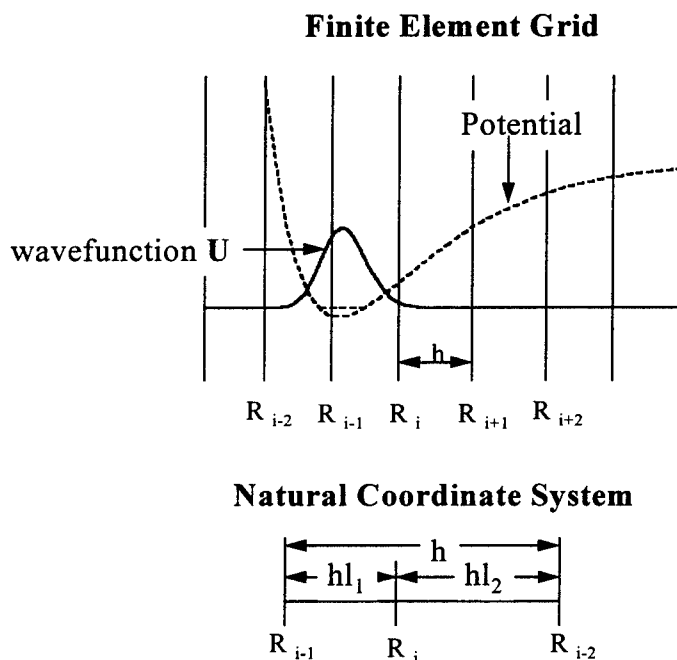


Figure II-7. This diagram depicts the Finite Element Grid and Natural Coordinate System. The wavefunction and potential's value and slope are approximated at each gridpoint R_i . The stepsize of each element is h . The stepsize does not necessarily have to be constant, but for the algorithm developed here, h is constant. The natural coordinates l_1 and l_2 are introduced to ease the integration later on.

The following relationships are true for the natural coordinate system

$$\begin{aligned}
 R &= R_i + l_2 h, \\
 R &= R_{i+1} - l_1 h, \\
 h &= R_{i+1} - R_i, \\
 l_1 + l_2 &= 1
 \end{aligned}
 \tag{II-27}$$

where R_i is the location of the i th grid point, and l_1 and l_2 are the natural coordinates.

The finite element method converges as long as the requirements for completeness and compatibility are satisfied (16:114-115;15:22). Namely, the value of U and its slope must be continuous at each grid point. Therefore, U can be approximated at the local element to be

$$U^e(R) = U^e(l_1, l_2) = U_0 f_1(l_1, l_2) + U_0' f_2(l_1, l_2) + U_1 f_3(l_1, l_2) + U_1' f_4(l_1, l_2) \tag{II-28}$$

where the superscript e means this formula is only valid for the local element in question.

U_0 and U_1 are constants which have values of wavefunction located at the endpoints R_i

and R_{i+1} . U_0' and U_1' are constants which represent the slope of U at R_i and R_{i+1} ,

respectively. The interpolating polynomials, f_{1-4} , turn off and on in order for Equation II-

28 and the derivative of this equation to meet boundary conditions. For example,

$U^e(R=R_i)$ should equal U_0 , and $U^e'(R = R_{i+1})$ should equal U_1' , etc.

Since, $V(R)$ is required for the integration of Equation II-26, in a similar fashion as this, it is also approximated.

The natural coordinates are then used to build the interpolating functions as cubic polynomials. The basis set for cubics in l_1 and l_2 is $\{l_1^3; l_1^2 l_2; l_1 l_2^2; l_2^3\}$. The cubic interpolating functions are then substituted into Equation II-26. Now the integrals are simple polynomials completely in terms of l_1 and l_2 , and the constants U_0 , U_0' , U_1 , and U_1' . Using the formula (17:37; 15:25)

$$\int_0^h l_1^p l_2^q dl_1 dl_2 = \frac{h p! q!}{(p+q+1)!} \quad (\text{II-29})$$

computing the integrals becomes straight forward and trivial. As an example, the first integral in the numerator of Equation II-26 (after some clever manipulation) evaluates to

$$\left\langle \frac{\partial U}{\partial R} \middle| \frac{\partial U}{\partial R} \right\rangle^e = \begin{bmatrix} U_0 & U_0' & U_1 & U_1' \end{bmatrix} \frac{1}{240h} \begin{bmatrix} 144 & 12h & -144 & 12h \\ 12h & 16h^2 & -12h & -4h^2 \\ -144 & -12h & 144 & -12h \\ 12h & -4h^2 & -12h & 16h^2 \end{bmatrix} \begin{bmatrix} U_0 \\ U_0' \\ U_1 \\ U_1' \end{bmatrix} \quad (\text{II-30})$$

In a similar manner, the rest of Equation II-26 is tackled. The second integral in the numerator, which includes the potential energy, breaks apart into four separate integrals.

Therefore, including the denominator, six different integrals are evaluated and manipulated into forms similar to Equation II-30. For complete details see reference 15. An important note, these matrices are a consequence of the finite element method, and should not be confused with matrices found in the formalization of quantum mechanics.

Now that each of the six integrals have been transformed into matrices for the local element only, it's now time to assemble the global system. This equation is the matrix system which represents the entire grid, not just the local element. Each local element has a neighboring element on either side. Therefore, the boundary values of each element (its edges) should match its neighbor. With this in mind, a global matrix can be assembled by overlapping the matrices on top of each other. See Figure II-8 to see how this is done.

Building the Global Matrix

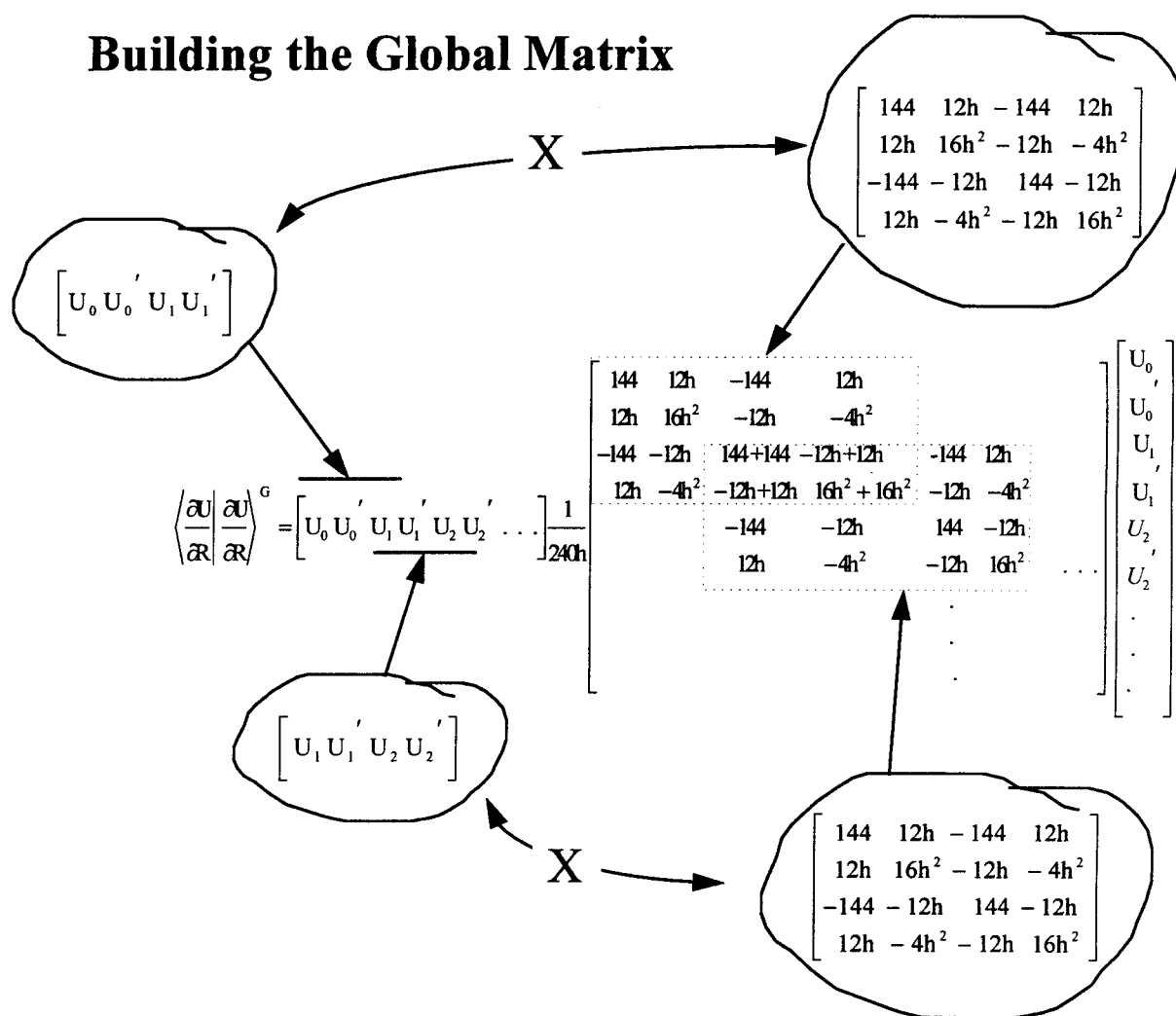


Figure II-8. This figure illustrates how the global finite element matrix is assembled. Each grid element consists of two endpoints. At each endpoint, the unknowns are the wavefunction value and its slope. Hence, that's four unknowns. But, each element has a neighbor to each side, and at these common boundaries their functional values need to match. Therefore, each local matrix overlaps with its neighbors matrix. See Equation II-30 for a sample matrix equation which could represent the element. This diagram, however, only depicts the first two elements being overlapped. The building process actually continues until every grid element has been included. Notice the square matrix is banded, it consists of one main diagonal plus three lower and upper diagonals. Therefore, the vast majority of its elements are zero. The "X" in the diagram indicates matrix multiplication.

For simplicity, Figure II-8 only shows the global matrix being built for one integral. Remember, there are five other integrals to do. Five integrals are summed together in the numerator and manipulated into a form similar to Equation II-30 which is just one of these five integrals. The denominator is fashioned in a similar way.

If we identify the column vector (this contains the unknown U and U' values) as \mathbf{Z} , the square matrix in the numerator as \mathbf{H} , and the square matrix in the denominator as \mathbf{S} Equation II-26 becomes

$$E = \frac{\mathbf{Z}^T \mathbf{H} \mathbf{Z}}{\mathbf{Z}^T \mathbf{S} \mathbf{Z}} \quad (\text{II-31})$$

In summary, \mathbf{Z} contains information about the wavefunctions, \mathbf{H} describes the energy, and \mathbf{S} contains information about the grid. The \mathbf{S} matrix is a normalization operator.

To find the eigenvalues and eigenvectors, the \mathbf{H} matrix needs to be diagonalized. However, this form does not lend itself immediately to an eigenvalue problem. Therefore, Equation II-31 is manipulated into

$$\begin{aligned}
\mathbf{H}\mathbf{Z} & - \mathbf{E}\mathbf{S}\mathbf{Z} = 0 \\
\mathbf{H}\mathbf{Z} & - \mathbf{E}\mathbf{L}\mathbf{L}^T\mathbf{Z} = 0 \\
\mathbf{H}(\mathbf{L}^T)^{-1}\mathbf{L}^T\mathbf{Z} & - \mathbf{E}\mathbf{L}\mathbf{L}^T\mathbf{Z} = 0 \\
\mathbf{L}^{-1}\mathbf{H}(\mathbf{L}^T)^{-1}\mathbf{L}^T\mathbf{Z} & - \mathbf{E}\mathbf{L}^{-1}\mathbf{L}\mathbf{L}^T\mathbf{Z} = 0
\end{aligned}
\tag{II-32}$$

$$\mathbf{X}\mathbf{Y} - \mathbf{E}\mathbf{Y} = 0$$

where $\mathbf{X} = \mathbf{L}^{-1}\mathbf{H}(\mathbf{L}^T)^{-1}$ and $\mathbf{Y} = \mathbf{L}^T\mathbf{Z}$, and $\mathbf{L}\mathbf{L}^T$ is the Cholesky decomposition of \mathbf{S} (15:32-35).

\mathbf{X} has the same eigenvalues as \mathbf{H} . Therefore, the eigenvalues can be immediately found by diagonalizing the matrix \mathbf{X} . The diagonalization is easily done with “off the shelf” math routines (see Chapter 3). Recovery of the eigenvectors, on the other hand, requires an extra step. The eigenvectors are simply related to \mathbf{Y} , that is, $\mathbf{Z} = (\mathbf{L}^T)^{-1}\mathbf{Y}$. The eigenvectors are normalized by the relationship $N^2 = \mathbf{Z}^T\mathbf{S}\mathbf{Z}$, where N is the normalization factor.

The rank of the matrices goes as $m = 2(ne+1)$, where m is the rank of the matrix, and ne is the number of elements. Therefore, when \mathbf{X} is diagonalized m eigenvalues will be found. Also, \mathbf{Z} (which contains the eigenvectors) is an $m \times m$ matrix. Each column of \mathbf{Z} is an eigenvector, where each column contains $(ne+1)$ pairs of data. This data is the eigenfunction's value and slope at each gridpoint.

The accuracy of this solution is related to the number of elements. As the number of elements increases the stepsize decreases (assuming the endpoints of the grid are fixed). The convergence is (14:37-38)

$$\boxed{|e(x)| \leq c h^{n+1}} \quad (\text{II-33})$$

where $|e(x)|$ is the residual between the exact solution and the numerical solution, c is a constant, h is the stepsize, and n is the order of the interpolation polynomial. Hence, for cubic elements, the error decreases as order h^4 .

An interesting consequence of this solution, is that the number of elements must be increased to decrease the stepsize h in order to increase the accuracy of the solution,. However, as the number of elements is increased, so do the number of eigenvalues and eigenfunctions calculated.

Now that the eigenfunctions have been found, the Franck-Condon Factors can be calculated.

Conclusion

This chapter showed how the knowledge of Einstein's Coefficients are vital to transition analysis and laser engineering. Einstein's Coefficients can be derived through

the relation of Franck-Condon Factors. However, these factors are only revealed if the molecule is known intimately, namely through its eigenfunctions which describe the nuclear motion. Morse found the eigenfunctions analytically for a potential energy curve similar to a molecule. Unfortunately, this model is adequate only for the lowest bound states of molecules

The SDO method showed how Schrödinger's Equation can be solved numerically for an arbitrary potential, $V(R)$. But, if $V(R)$ is not known for the molecule, how do you solve for the molecule's eigenfunctions?

The next chapter, Computer Modeling, describes how the SDO method exhaustively solves Schrödinger's Equation over and over again hunting down that elusive $V(R)$. Once, a good representation of $V(R)$ is found, the eigenfunctions are computed.

III. Computer Modeling and Programs

Introduction

This chapter describes how the SDO method is implemented on a computer to calculate the Franck-Condon Factors. Contrary to the emphasis of the previous chapter, the most important feature of the SDO method is how it searches and finds the “best” potential curve for the molecule in question. Thereby, knowing the potential, the wavefunctions can be calculated with the method of finite elements, which lead to the Franck-Condon Factors.

Experimental spectroscopic data is central to the search for the “best” potential. First, this chapter explains how this transition data needs to be presented to the computer model. Next, a description explains how this spectroscopic data is used in the hunt, that is, the search for the “best” potential. Followed by a section which describes how to run the code which includes execution strategies. And finally, once the potential curve has been identified, how to numerically calculate the Franck-Condon Factors.

Background of Computer Models

The vast majority of this research effort was spent fixing, changing, creating, and testing FORTRAN code. This section documents these efforts. The specific details of these codes is discussed later.

Four major FORTRAN codes previously written in 1984 (2) were used for this project. Unfortunately, these codes survived only on paper. Therefore, the codes were either typed in by hand or scanned in with a machine. Neither of these processes worked all too well. A great deal of time was spent searching for bothersome bugs created by typos and mistakes, and some were not obvious. To add to the confusion, the FORTRAN compiler used for this project interpreted some of this old code differently. Again, more modifications had to be made to make the code work as intended.

Several of the commercial subroutines used by these programs no longer existed and/or were missing. These routines included IMSL Math/Library® functions and a non-linear minimization routine (5). Both of their intended functions are discussed later in detail.

After 1984, IMSL decided to completely revamp their libraries. This meant the algorithms previously used did not exist any more. In fact, much of the code previously written had been specifically adapted to use these missing routines. These adaptations mainly included matrix storage modes compatible with these math routines. Therefore,

not only did new IMSL routines have to be figured out, but the old matrix storage modes within the code had to be re-written.

Why bother with these IMSL routines in the first place? The purpose for using the IMSL math routines is simple. This code requires large matrix manipulations and calculations. Due to the complexities of this math, such as diagonalizing a 1500x1500 matrix, this commercial product was selected to avoid any possible math problems.

The non-linear minimization routine used by the main program no longer existed in digital format either. This routine, acquired from Professor Pearson of the University of Washington, is an older code written before modern programming conventions became standard. This situation created run-time errors that were not initially anticipated.

Further, new code and subroutines were written to handle unforeseen complexities encountered with this research. The code previously depended on a rigid placement of the finite element grid. However, convergence problems were discovered with this approach. Therefore, a new algorithm was written to adaptively change the grid during code execution. Another grid problem was discovered when calculating the Franck-Condon Factors. These overlap integrals require the same grid be employed for two distinct executions of the code. A new subroutine was written to ensure these two grids coalesced, even sliding one of the grids if needed.

Countless other small coding changes were also made. These included improved output listings and re-dimensioning of variables to handle larger matrices.

The rest of the chapter now focuses on a detailed discussion about these four main programs. The remaining sections include explanations about some of the algorithms, “how to run” the codes, and execution strategies.

Preparation of Spectroscopic Data

To find the best potential surface which describes the molecular forces, experimental spectroscopic data must be supplied to the model. This spectroscopic data is used as the benchmark for the model to decide which potential "best" matches the molecule. This spectroscopic data must be presented in a vibrational eigenvalue format for each electronic state of interest.

To develop the vibrational eigenvalues, the experimental spectroscopic data can be furnished in either of two forms. The first form, and the most obvious, is a listing of the actual observed emission or absorption lines of the molecule. The other acceptable way is to offer the spectroscopic data in terms of the Dunham Coefficients.

In 1932, Dunham devised a formula which compactly describes the energy of a rotating vibrator in terms of coefficients (1). His formula is

$$F_{vK} = \sum_{ij} Y_{ij} \left(v + \frac{1}{2} \right)^i K^j (K+1)^j \quad (\text{III-1})$$

where F_{vK} is the energy (the eigenvalue) of the rotating vibrator, v is the vibration level, K is the rotational level, and Y_{ij} are the Dunham coefficients.

Therefore, if the Dunham coefficients are known for a given electronic state of the molecule, then the energy eigenvalues can be calculated. Often, these coefficients are reported in journal articles in lieu of the actual spectroscopic data.

Ostdiek developed a FORTRAN code (2: 5-6, 44-48, A1, B1-B8), called *dunham*, which automatically calculates the energy eigenvalues given these coefficients as input.

Figure III-1 illustrates a sample input file for the program *dunham*.

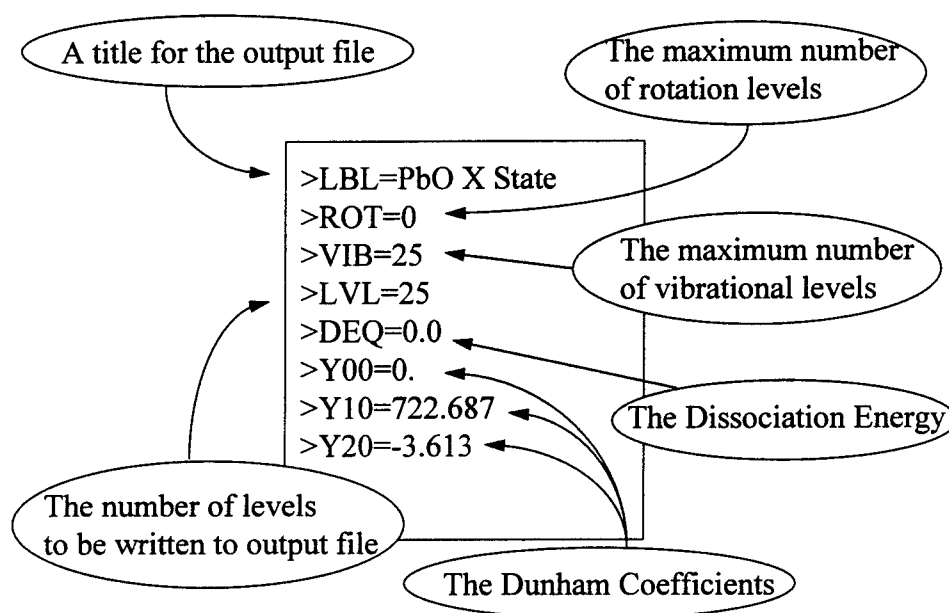


Figure III-1. This figure illustrates a sample input file for the Dunham software (2:47). This example only gives the first three Dunham coefficients for the ground electronic state of PbO. The accuracy of the energy eigenvalues can be increased by supplying more Dunham coefficients. Since, the rotational fine structure is not needed, *ROT* is always set to zero. The output of *dunham* are vibrational eigenvalues for the electronic state of interest.

A second FORTRAN code, called *efit* (2: 6-14, 48-54, C1-C2, D1-D13), takes observed vibronic transition data and fits the data into an eigenvalue form. This code provides an alternative method over *dunham*. The observed spectra from diatomic molecules often are the electronic transitions. Within these transitions is buried the vibrational structure. This structure, or splitting of the lines, is measured with a monochromator or some similar device. The eigenvalues can then be determined by some differencing techniques using these observed spectral lines. Figure III-2 demonstrates this point. The figure shows three vibronic transitions, all from a common upper vibrational level. When illustrated such as this, clearly two of the lower vibrational eigenvalues can be determined by differencing the observed transitions.

Molecular Transitions

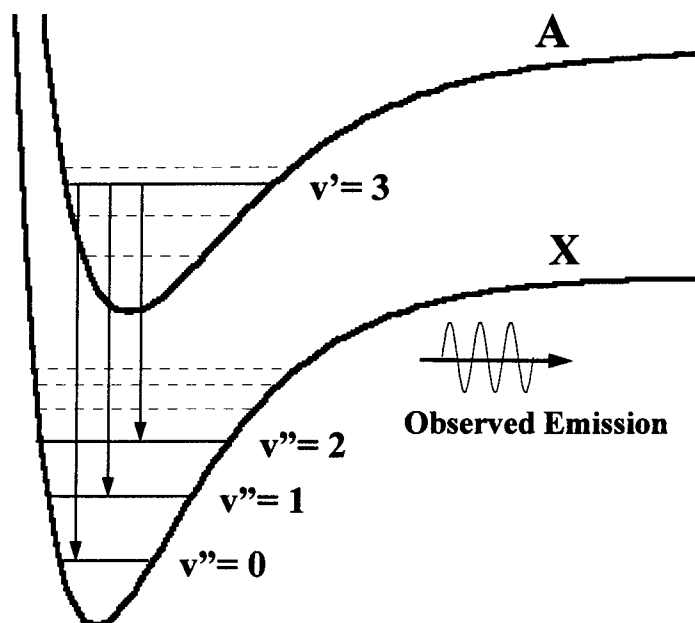


Figure III-2. This figure illustrates vibronic transitions of diatomic molecules. In this example, electronic state *A* is transitioning to the ground state labeled *X*. The observed spectrum is indicative of the energy difference between the levels. If the transitions can be identified as to which are taking place, such as $v'=3$ to $v''=0$, then the vibrational eigenvalues of each state can be determined. For clarity, only three transitions are illustrated here. A simple differencing method could be employed to garner the first two eigenvalues of the ground state. The output of *efit* is a list of the vibrational eigenvalues for each electronic state used for the fit.

Due to measurement error and uncertainty in the data, several transitions may indicate different values for the same eigenvalue. Obviously, this can't be true. The program *efit* uses a least squares fit to resolve these inconsistencies between the data. A transition line involving one energy level is, therefore, made to agree with other transitions lines involving the same energy level. (2: 8-9) This correction is obtained by minimizing the sum

$$S = \frac{1}{2} \sum_{i=1}^p \sum_{j=1}^p w_{ij} (l_{ij} - \epsilon_i + \epsilon_j)^2 \quad (\text{III-2})$$

where S is the sum to be minimized, w_{ij} is the weighting factor, l_{ij} is the observed transition line between state i and j , ϵ_i and ϵ_j are the eigenvalues of state i and j , respectively.

This program can accept up to 62,500 transition lines, involving 250 energy levels from 10 different electronic states. Figure III-3 illustrates for a sample input file for the program *efit*.

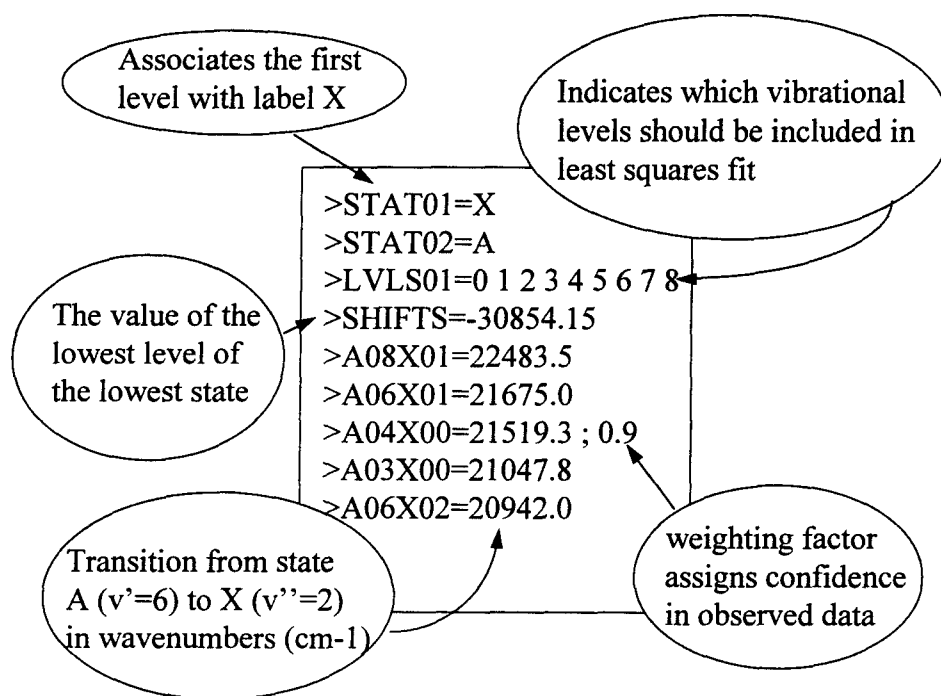


Figure III-3. This figure illustrates the input file for the program *efit*. This sample input file should not be taken literally, a real input would include more transitions than indicated here. The user specifies the energy for each transition with its assignment. The weighting factor defaults to 1.0 if none is specified. The output of *efit* is the energy eigenvalues for each electronic state used during the fit.

Now that the eigenvalues have been determined for each electronic state, it is now time to find the “best” potential which describes this state.

The Hunt

The program *diatom* is responsible for hunting down the “best” potential surface. The “best” potential is identified by finding the potential surface which yield numerical eigenvalues which are the closest to the experimental data (2: 54-84, E1-E2, F1-F44). But before the procedure for executing *diatom* is explained, some background information about this algorithm must first be addressed. For a complete description of *diatom*'s input files, and execution strategies see the next section, *Executing the Code*.

This background material includes a discussion about the iterative hunting process, the parameterized potential functions, the non-linear minimization routine, and automatic gridding.

The program *diatom* uses a non-linear minimization routine to find the “best” potential curve. The minimization routine accomplishes this by adjusting parameters of a selected potential function. Then to test its hypothesis, Schrödinger's Equation is solved with the finite element method using for this potential curve with these new parameter values. (see Chapter II). The difference between the computed and experimental eigenvalues then is used to provide feedback to the minimization routine. This process is repeated exhaustively until the optimum potential surface has been found

The following equations lists the parameterized potential functions which are available to *diatom* and the user. These functions model the vibrational energy forces only. The rotational energy is not modeled with this finite element method (see Chapter II), nor do the following equations capture the rotational energy. The parameters of these function are what the minimization routine adjusts in its search for the global minimum.

$$V(R; k) = \frac{1}{2} k (R - R_e)^2 + T_e \quad (\text{Harmonic})$$

$$V(R; D_e, a) = D_e \left(\left(1 - e^{-a(R-R_e)} \right)^2 - 1 \right) + T_e \quad (\text{Morse})$$

$$V(R; D_e) = D_e \left(\left(\frac{R_e}{R} \right)^{12} - 2 \left(\frac{R_e}{R} \right)^6 \right) + T_e \quad (\text{Lennard - Jones}) \quad (\text{III-3})$$

$$V(R; D_e, \alpha, \beta) = D_e \frac{\beta}{\alpha - \beta} \left(\left(\frac{R_e}{R} \right)^\alpha - \frac{\alpha}{\beta} \left(\frac{R_e}{R} \right)^\beta \right) + T_e \quad (\text{Mie})$$

where V is the potential function, R is the internuclear separation, k is the harmonic force constant, R_e is the equilibrium distance, D_e is the dissociation energy, a is the Morse anharmonicity term, α and β are exponents in the Mie potential, and T_e measures the energy separation between the minima of the two electronic state potential energy curves. (3:136). The adjustable parameters are k , D_e , a , α , and β .

The Harmonic and Morse functions are the only functions listed in Equation III-3 that have known analytic solutions. They were explicitly included in this list for this very

reason. Their solutions are discussed in Chapter II and are invaluable for the validation process. For more information about the validation process see Chapter IV.

Next on the list is the Lennard-Jones potential. The Lennard-Jones potential is cleverly constructed to take advantage of the fact that van der Waals' intermolecular attractive forces go as R^{-6} . This attraction is a "self-generating boot-strap force", called the London dispersion force. The London dispersion force is caused by the fluctuating electron density of each molecule. In effect, a temporal dipole moment from one molecule induces a dipole moment on a neighboring molecule, which in turn induces back (4: 52-54,115-117). The repulsive branch, modeled by the R^{-12} term, has no physical foundation. This repulsion term was chosen as a mathematical convenience to ensure the minimum of this potential occurs at R_e .

The Mie potential is formed when both exponents of the Lennard-Jones potential are parameterized. Most molecular forces don't exactly go as R^{-6} and R^{-12} . By varying these exponents, the Mie potential can be adapted to match these actual forces. Both the attractive and repulsive branches of the Mie can be varied independently, unlike the others. Therefore, the Mie potential is the most flexible of the potentials listed in Equation III-3. The additional coefficients ensure the minimum of this potential remains at R_e . With a few algebraic substitutions, the Morse and Lennard-Jones potentials can be shown to be special cases of the Mie potential (2: 17).

The equilibrium distance, R_e , and the energy separation, T_e , are not variable parameters. Within *diatom*, these values are treated as constants. Since this analysis does not include the rotational fine structure, R_e must be supplied by the user. T_e must also be

supplied by the user. T_e is defined as zero for the ground electronic state. For details on how to calculate these values see the section labeled *Executing the Code*.

For the potential selected by the user, the minimization routine (5) adjusts the potentials parameters in a systematic manner. First, the eigenvalues are computed for an initial “guess” of the parameters in question. Then, the sum of residuals squared is calculated by differencing the experimental eigenvalues (the bench mark) and the newly computed eigenvalues. The formula used is

$$\text{Sum} = \frac{1}{2} \sum_{i=1}^n w_i \left(E_{\text{experimental}}^i - E_{\text{calculated}}^i \right)^2 \quad (\text{III-4})$$

where w_i is the weight factor, $E_{\text{experimental}}^i$ is the observed eigenvalue, $E_{\text{calculated}}^i$ is the computed solution, and n is the maximum number eigenvalues furnished by the user. The minimization routine then adjusts the parameters of the chosen potential (hopefully in the direction to the global optimum), the eigenvalues are then re-computed, the sum of residuals squared is recomputed, and so on. This process is exhaustively repeated until the sum of the residuals squared has been minimized, thereby, the “best” solution has been isolated. See Figure III-4.

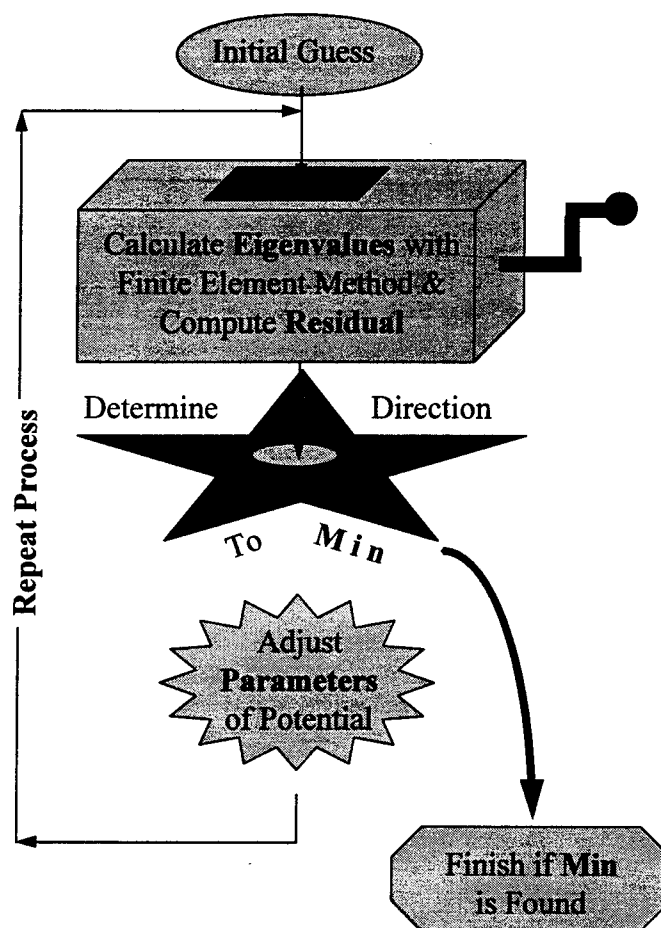


Figure III-4. This figure illustrates schematically the iterative hunting process. From an initial starting place given by the user, the model computes the vibrational eigenvalues using the method of finite elements. The sum of the residuals squared is then computed (See Equation III-4) and the non-linear minimization routine then determines which direction must be made to find the minimum. The minimization routine then adjusts the parameters of the potential accordingly, and reseeds the process. The process is complete when the global minimum has been found, that is, the best potential which yields the eigenvalues closest to experimental results.

This non-linear minimization routine searches for the global minimum of an N-dimensional parameter space by making a series of gradient steps, random direction steps, average directional steps, and random jumps within the parameter space. This program uses the method of steepest descents for its gradient maneuvers. If the routine hits a

boundary of the parameter space it will "slide" along the boundary until improvement ceases. The random jumps ensure the routine does not fall into a local minimum, thereby, missing the global optimum.

The parameter space in which this minimization routine searches for the global optimum is graphically shown in Figure III-5. This surface was generated by calculating the sum of the residuals squared for over 1000 points. The analytical eigenvalues of the Morse Oscillator were provided as the benchmark for a dissociation energy (D_e) of 15000.0, and an anharmonicity term (a) of 6.0. Then the sum of the residuals squared was calculated as a was varied from 1.0 to 12.0, and D_e was varied from 6000.0 to 24000.0. The height of the surface in Figure III-5 is the log of the sum of residuals squared at each (a , D_e) coordinate pair. This height was then truncated so the lowest value was 6. This truncation was done in order to see more resolution in the plot.

The graph shows some very important features of this parameter space. The most important feature is that there is only one minimum. And this minimum is extremely pronounced. Another feature is that the surface which the minimization routine moves upon appears smooth, for the most part. A gradient search method should be sufficient to find the global minimum for a surface such as this. The two triangular bumps are real and were calculated independent of each other. The origin of these bumps is not currently understood.

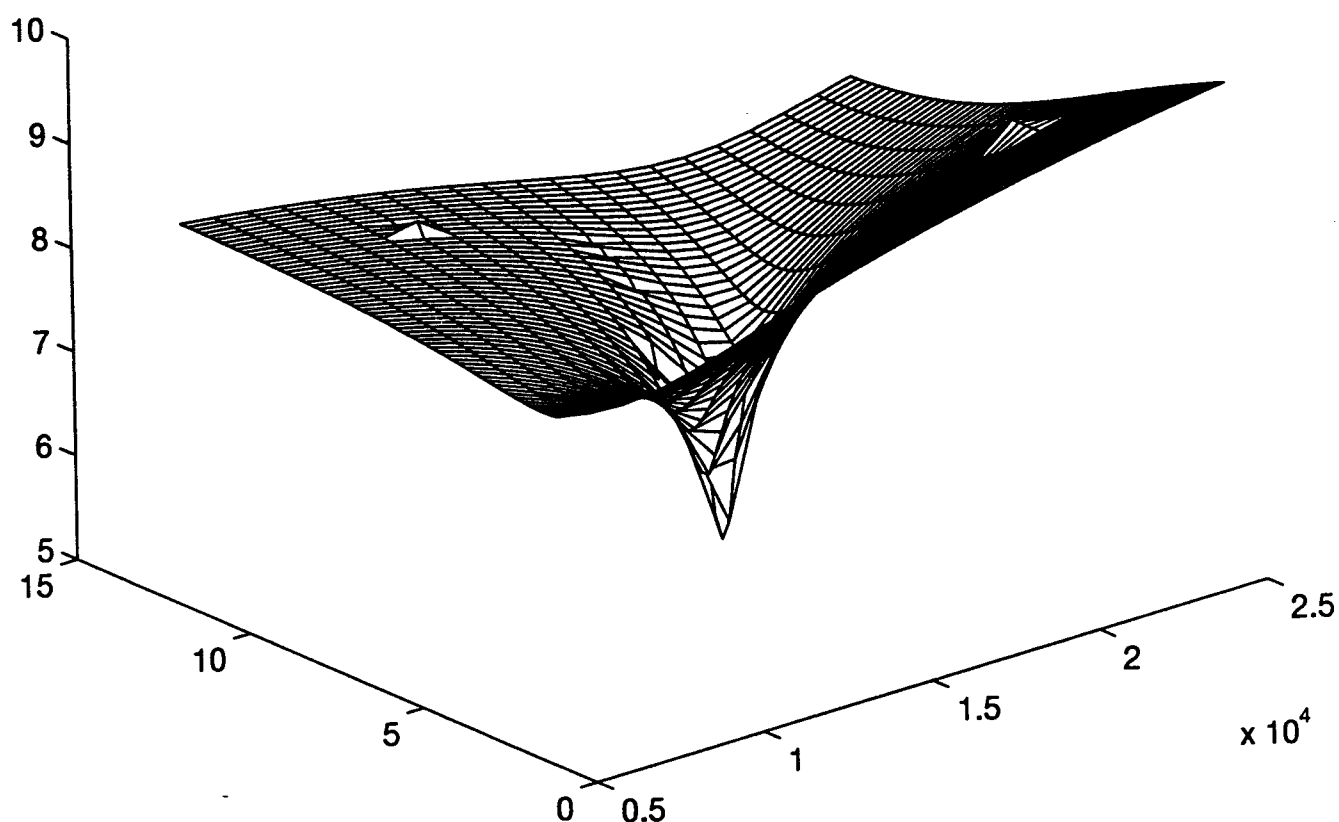


Figure III-5. This figure illustrates the parameter space for where the hunt occurs. The minimization routines roams around on this surface until it finds the global optimum. The analytical solutions of the Morse potential where $a=6.0$ and $D_e=15000.0$ were provided as the benchmark. This benchmark included all 28 bound states. The height of this surface represents the order of magnitude (log scale) of the sum of residuals squared (i.e. a measure of how close the computed eigenvalues are to the benchmark). The sum of the residuals squared was computed for a from 1.0 to 12.0 (the x-axis), and for D_e from 6000.0 to 24000.0 (the y-axis) for 300 grid elements. The bottom of this well's order of magnitude is actually 10^1 , it was truncated at 10^6 for illustrative purposes. Another important point, because this is an order of magnitude graph, subtle changes in value may be washed out. The two triangular bumps were calculated independent of each other.

The math routines which diagonalizes \mathbf{H} matrix (see Chapter II) are two IMSL® Math/Library™ FORTRAN subroutines (6: 307-311). The first routine, *DEVLSF*, computes the eigenvalues of a real symmetric matrix by an orthogonal similarity transformation to an equivalent symmetric tridiagonal matrix, then it performs an implicit

QL algorithm to compute the eigenvalues of this matrix. The second routine, *DEVCSF*, does the same thing, but also returns the eigenfunctions. These eigenfunctions are normalized such that the infinity norm of each vector is one.

The important point here is, while the minimization routine is hunting for the best potential, *DEVLSF* is the routine that is used to compute the eigenvalues. This saves time because *DEVLSF* works faster than *DEVCSF*. Once the best potential has been found, then *DEVCSF* is called to calculate the eigenfunctions. Therefore, *DEVCSF* is only called once at the very end of execution.

In the original version of *diatom*, the user had complete control over the finite element grid. The user specified where the two grid endpoints were located, and the number of elements to be used. Once the grid was defined, however, this grid was used for all calculations, no matter how the minimization might adjust the parameters of the potential. Refer to Figure II-7.

The convergence of the finite element method, as it turned out, is very sensitive to how the grid was laid down. See Chapter IV for a discussion on convergence. For example, if the endpoints of the grid were positioned so that only a small part of the potential was included for the calculation, the solution would not converge. This situation is easily obtained. Recall the global minimization routine adjusts the parameters of the potential function. And these adjustments may be systematic or even random. Therefore, the potential curve may swing completely off a previously defined grid.

Therefore, the program *diatom* has been modified in this work to automatically adjust the grid during execution for the user. The endpoints of the grid are adjusted so

that the potential curve, and the bound state wavefunctions do not get truncated by the grid endpoints as the minimization adjusts the parameters of the potential function. This smart grid algorithm automatically “walks the endpoints in and out” every time the potential function’s parameters are changed by the minimization routine.

The endpoints are adjusted so that the value of the potential satisfies certain conditions. The value of the repulsive branch at the left endpoint must fall between 10 times and 1000 times D_e . The value of the attractive branch at the right gridpoint must fall between -10^{-4} and -10^{-6} times D_e . These values were chosen from experience and experiment. Other than the fact these limits work, they were chosen arbitrarily.

Executing the Code

This section does two things. First, the input files are explained in detail. Second, execution strategies are discussed.

The program diatom requires two input files for execution. One input file defines the bench mark for the best potential, that is the experimental vibrational eigenvalues for the electronic state of interest. The second input file is a master control file which manages the execution.

Figure III-6 shows a sample eigenvalue energy input file.

diatom_energy.input

```
>LBL=MORSE: De=15000 cm-1, a = 6.0  
>V00=-14484.8847577293  
>V01=-12481.6542731880  
>V02=-10687.9628195640  
>V03=-9828.7323350227  
.  
.  
.  
>V23=-518.58361327  
>V24=-343.35312  
>V25=-204.122644196  
>V26=-100.8921596549  
>V27=-33.6616751135  
>V28=-2.4311905722
```

**Title to be Included
in Output**

**Vibrational Energy
Eigenvalue at v=5**

Figure III-6. This figure illustrates the energy input file for diatom ("diatom_energy.input"). This file defines the benchmark for the best potential. The model will attempt to find a potential whose eigenvalues match most closely to these. As an example, this list includes the 28 analytical eigenvalues for a Morse Oscillator where $a=6.0$ and $D_e=15000.0$. The format for each energy input is ">Vxx", where xx is the state label. Labels less than 10 still must have digits, such as ">V05".

Figure III-7 shows the master control input file.

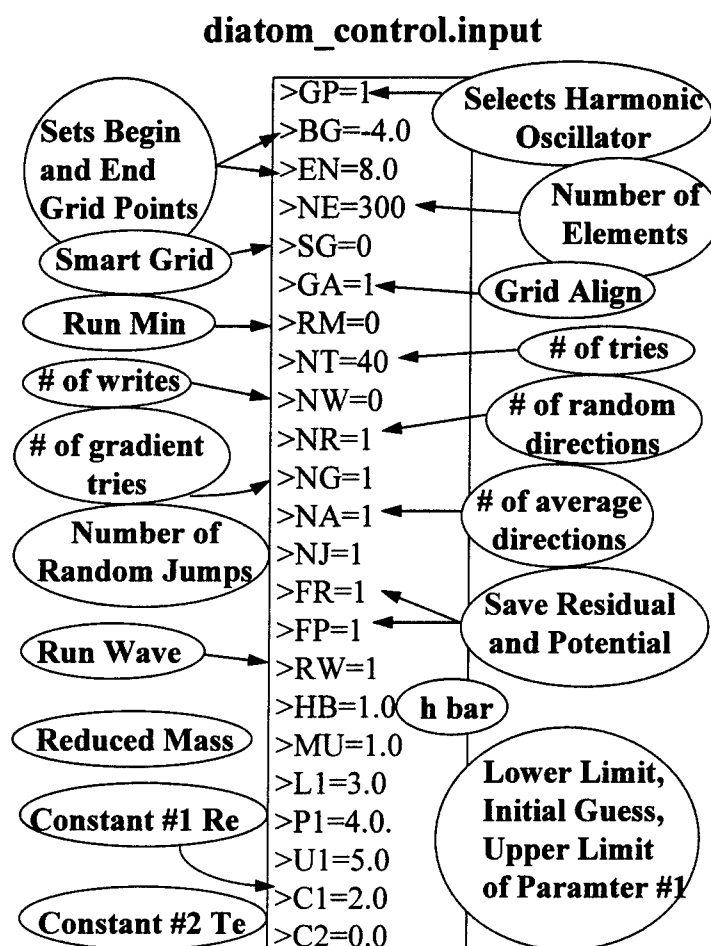


Figure III-7. This figure illustrates the master control input file for *diatom* ("diatom_control.input"). This file's syntax is ">AA=" where AA is a two letter code. All of the possible codes are exemplified in this sample. This input files consists of three main groups. The first group controls the grid, the second group controls the minimization routine, and the third group controls the potential and its associated parameters and constants. The two letter code, RM, turns the non-linear minimization routine on and off.

The two letter code **GP** selects the generalized potential as shown Table III-1.

Table III-1. This table shows how to select the GP flag.

Potential Function	GP value
Simple Harmonic Oscillator	1
Morse Anharmonic Oscillator	2
Lennard-Jones Potential	3
Mie Potential	4

Each potential function has a number of parameters and constants (refer to Equation III-3). The user has the ability to define a search space for each parameter. That is, define the upper and lower limits for each parameter, and define its initial starting value. These values define the parameter space where the minimization routine hunts for the best potential.

Table III-2. This table shows the relationship between the parameter and constant variables, and the numbers they are identified by in the control input file.

Potential	Parameter 1	Parameter 2	Parameter 3	Constant 1	Constant 2
Harmonic	k	-	-	R_e	T_e
Morse	D_e	a	-	R_e	T_e
Lennard-Jones	D_e	-	-	R_e	T_e
Mie	D_e	α	β	R_e	T_e

For example, the lower limit, upper limit, and initial value of a (Morse's anharmonicity term) would be denoted by the codes L2, P2, and U2, respectively. See Figure III-7 for the example input file.

Optimally, the user wants to initialize the parameters as close to the expected values as possible. This preemptive measure will help the search routine find the "best" potential sooner. Also, set the lower and upper limits as tight as possible. This will limit the search volume, and again speed things up. Later, Chapter IV will show that solutions of acceptable accuracy require a lot of elements, which translates into lots of time. Some quick estimates of the solution can be extremely beneficial.

Since this analysis does not include the rotational fine structure, R_e must be supplied by the user. The equilibrium distance, R_e , can be computed by using the rotational spectral constant B_e . T_e may be approximated by finding the difference between the ground vibrational eigenvalue of the upper electronic state and the ground vibrational eigenvalue of the ground state. However, a preferable solution is to calculate

T_e by subtracting $\frac{1}{2}\omega_e - \frac{1}{4}\omega_e\chi_e$ from the ground vibrational eigenvalue of each

electronic state, and then subtracting these two values. This method assumes the potential energy curve behaves like a Morse Oscillator at the bottom of the well, which in most cases is a good approximation. Again, ω_e and $\omega_e\chi_e$ are vibrational constants.

The grid is controlled by five settings. The settings, **BG** and **EN**, position the left and right grid endpoints respectively. These values have dimensions of length. The setting **NE** carves up the grid into the number of elements specified, all of equal size.

The setting **SG**, the smart grid algorithm, has three settings. Setting this parameter to 0 turns it off, 1 and 2 turns it on. With **SG** turned on, the smart grid walks the grid endpoints in and out as needed to keep the grid space defined properly for the potential curve in question. With **SG** set to 1, the initial stepsize is kept constant, therefore, the number of elements vary as the endpoints are adjusted. With **SG** set to 2, the number of elements is kept constant, therefore, the stepsize varies as the endpoints are adjusted. The setting **GA**, the grid alignment algorithm, co-aligns grids of separate executions. Setting it to 0 turns it off, and setting it to 1 turns it on. This algorithm records previously defined grids by writing data to a special output file. This information is then used to align the grids. The grid alignment algorithm must be turned on if the eigenfunctions are going to be used for Franck-Condon calculations. Note, turning the grid alignment on overrides the smart grid assignment of 2, switching it to 1.

The non-linear minimization routine has 7 settings to control its execution. The flag **RM** turns the minimization routine on and off with 1 and 0, respectively. If the minimization routine is off, the code will calculate the eigenvalues for the initial parameter settings only. When on, the minimization routine will make **NT** number of attempts to find the global minimum. The flags **NR**, **NG**, **NA**, **NJ** control the relative number out of **NT** tries each of these strategies will be attempted. The setting **NR** controls the number of times it tries a random direction looking for the minimum, **NG** is the number of times gradient steps should be taken, **NA** is the number of average directions it should take, and **NJ** is the number of times it should take a random jump to some other point in the parameter space. **NW** controls the number of times it reports

diagnostic information to the screen. It will never provide diagnostics if it is set to 0, but will report back every other step if the setting is 2, etc.

The designators **HB** and **MU** set the values of Planck's Constant over 2π (\hbar) and the reduced mass of the molecule. Units are important. The grid endpoints, **BG** and **EN**, **HB**, **MU**, and the energy eigenvalues all need to use the same unit system. Atomic units are recommended, because atomic units allow **HB** to be set to one, thereby, reducing numerical error introduced by using very small numbers. As an example, in SI units Planck's constant is on the order of 10^{-34} . Using such a small number could lead to significant numerical error, especially when using any algorithm to diagonalize matrices such as *DEVLSF*.

The last settings, **RW**, **FP**, and **FR** are option flags which turn on and off with settings of 1 and 0, respectively. **RW** instructs the diagonalization math routine to return both the eigenfunctions and eigenvalues. This setting saves time for the user when turned off if the user is not interested in the eigenfunctions. **FP** and **FR** instruct the model to save a potential and residual output file. The potential file contains 1000 coordinate pairs of position versus the value of the "best found" potential at each position. The residual file contains the listing of residuals for each experimental eigenvalue compared to its associated "best found" numerical eigenvalue.

A good strategy for running diatom is to start simple. Runs with lots of elements are expensive. The global minimization routine may solve Schrödinger's Equation hundreds of times depending on the execution and its input. Therefore, starting with a large search volume and a lot of elements could be costly. Start with not as many

elements, like a 150 or 200. As the minimization routine starts to hunt down the best potential, winnow the search volume. Also, run with the smart grid algorithm on. An initial setting of 2 will help control the number of elements used, and, therefore control time. The hunt for the best solution may take 5 to 10 runs, each run a refinement over the previous.

From experience, several of the minimization options should be turned off. These options include **NR** (random directions) and **NA** (average direction). Both of these options redirect the minimization routine away from the direction to the global optimum. Refer to Figure III-5 for justification of this recommendation. Figure III-5 suggests the parameter space is smooth and only one minimum exists. With this figure in mind, only gradient steps should be required to find this minimum. Random jumps to a new location in the parameter space may help avoid identifying the local minima as the global minima if they exist. The minimization routine identifies a minimum by comparing previous values. It could very well find a local minimum created by numerical noise. Therefore, the recommendations are to set **NR** and **NA** to zero, **NG** to 5, and **NJ** to 1.

The program *diatom* produces several output files. The first one is *diatom.output* which is the main output file. Another is *input_for_fcf.output*, this file contains the wavefunctions and S matrix required for the Franck-Condon Factor calculations. The last two output files are *plot_potential.output* and *plot_residual.output*. These files were described earlier.

Once the best potential has been found for both of the electronic states of interest, the Franck-Condon Factors can be calculated.

Franck-Condon Factor Calculations

This section describes how to calculate the Franck-Condon Factors with the program called *fcf* (2: 36-40, 66-70, G1-G2, H1-H10). This program uses the numerical wavefunctions obtained by executing *diamon* and its finite element method algorithm.

To calculate the Franck-Condon Factors, the overlap integral for every combination of upper electronic and lower electronic vibrational states must be computed. The eigenvectors garnered through the finite element method contain information about the wavefunction's value and slope at each gridpoint. However, this data just runs in successive order, and is not explicitly labeled for each gridpoint. Therefore, information about the grid is required to compute the overlap integral. This information is found in the **S** matrix as developed in Chapter II.

The Franck-Condon Factors are then calculated using the following formula:

$$q_{v'v''} = \left| \mathbf{v}'^T \mathbf{S} \mathbf{v}'' \right|^2 \quad (\text{III-5})$$

where $q_{v'v''}$ is the Franck-Condon Factor, v' is one of the wavefunctions for the upper electronic state, v'' is one of the wavefunctions for the lower electronic state, and S is the matrix which describes the grid space.

After a successful completion of *diatom* (with $RW=1$) the program automatically saves a file which contains the first 25 wavefunctions and the S matrix in the file *input_for_fcf.output*. Two of these output files are required for the Franck-Condon calculation, one for each electronic state. For this algorithm to work, both files must have the same S matrix. The automatic grid alignment algorithm ($GA=1$) must be invoked for both *diatom* runs to ensure they both have the same grid spacing. The S matrix, which depends on the number of elements and grid spacing, is adjusted to work for the largest wavefunction.

This grid alignment algorithm, new to *diatom*, does two things. One, it makes sure both runs have the same stepsize. And two, if the gridpoints are not co-aligned, this algorithm slides one of meshes over to coalesce with the other. In that way, both output files are ensured to have the same S matrix.

The FORTRAN program, *fcf*, takes these two output files (renamed by the user to *fcf_low.input* and *fcf_high.input*) and calculates the Franck-Condon factors. This program has been modified to handle wavefunctions derived from grids with different endpoints. The algorithm builds a 25x25 table of factors by looping over Equation III-5. The vector-matrix multiplication is carried out with two IMSL® Math/Library™ FORTRAN subroutines (6: 993-995). The first one is *DMURRV* which multiplies a real

rectangular matrix by a vector. The other is *DMURBV* which multiplies a real band matrix in band storage mode by a real vector.

The final output is the table of Franck-Condon Factors called *fcf.output*.

Conclusion

This chapter explained how starting with little information, namely some spectroscopic data, the Franck-Condon Factors can be calculated. The most important feature of this method, however, was not the calculation of the molecule's wavefunction which give you these factors. But, how it searched for and found the "best" potential curve for the molecule in question.

IV . Validation

Introduction

This chapter demonstrates that Schrödinger's Equation can be solved using the numerical method of finite elements. This validation includes comparisons between the analytical and numerical solutions of the Harmonic and Morse potentials. These sections are then followed by a discussion about the convergence of this method and its associated cost. And finally, the eigenvalues from a numerical H_2 molecule potential are used to demonstrate how the model can search and find an unknown potential.

Validation is an important effort for any model. No model should be trusted until it has the proven ability to predict known solutions accurately. Since the method of finite elements has not been used a lot in quantum mechanics, special emphasis is taken in this chapter to demonstrate the validity of this technique.

Simple Harmonic Oscillator

The harmonic oscillator is one of a few potentials known to have analytical solutions. The use of harmonic oscillator, therefore, is an obvious choice for validating any numerical solution of Schrödinger's Equation. This section details comparisons

between the analytical eigenvalues and functions, and their numerical equivalents computed with the method of finite elements.

The harmonic oscillator, as modeled in Equation III-3, was numerically evaluated using *diatom*. The force constant (k) was chosen to be 4.0, and the reduced mass (μ), $h/2\pi$, and the radius of equilibrium (R_e) were all set to 1.0 . The minimization routine was not used.

A finite element grid was laid down over this potential energy curve with the left endpoint at -5.0 and the right endpoint at 7.0 . This grid, therefore, is symmetric about R_e . A solution for 300 elements was arbitrarily chosen for this demonstration.

With the parameter choices listed earlier, the analytical eigenvalues conveniently become 1.0, 3.0, 5.0, and so on using Equation II-14. These values were then input to the *diatom* as the bench mark for residual calculations.

The residuals for the first 25 states yielded values on the order of 10^{-4} . That is, the difference between the analytical and numerical eigenvalues. The agreement demonstrated by the relative errors proved just as good. They ranged in value from 4.0×10^{-2} to 8.0×10^{-4} percent as shown in Table IV-1. This excellent agreement was found to be ubiquitous for all values of force constants and reduced masses tested.

Table IV-1. This table demonstrates the accuracy of the finite element method when solving Schrödinger's Equation for the Simple Harmonic Oscillator. For this test, $k=4.0$, $h/2\pi=1.0$, and $\mu=1.0$. A residual is defined as the difference between the expected and calculated eigenvalues.

Eigenstate Level	Calculated Eigenvalue	Residual	Relative Percent Error
0	1.000427	0.427E-03	0.427E-01
1	3.000427	0.427E-03	0.142E-01
2	5.000427	0.427E-03	0.853E-02
3	7.000427	0.427E-03	0.609E-02
...
22	45.000424	0.424E-03	0.941E-03
23	47.000412	0.412E-03	0.876E-03
24	49.000368	0.368E-03	0.751E-03
Sum of Residuals Squared		0.2245169E-05	

The sum of the residuals squared was on the order of 10^{-6} . For this comparison, the minimization routine had been turned off. However, if a search had been conducted, this value would have identified the global minimum.

The eigenfunctions also exhibited excellent agreement with the analytical solutions. These eigenfunctions were obtained using the following method. The *input_for_fcf.output* file contains a the listing for each eigenfunction. Eigenvectors for states 0, 1, 6, and 9 were then selected from this file. Two even states and two odd states

were chosen for their symmetry and asymmetry properties, respectively. Each vector is represented by a long column of numbers. This column is a sequential listing of pairs of numbers, each pair is the wavefunction's value and slope at each gridpoint, in successive order. For this analysis, only the wavefunction's value at each gridpoint was kept. The slopes were discarded.

These four eigenfunctions were then tested for proper normalization and orthogonality. All integrations were conducted using Simpson's rule. Normalization was tested by integrating each wavefunction squared over the finite element grid space. All four wavefunctions yielded a normalization factor of 1.0, even though only 7 significant digits were used to represent each point. Because these wavefunctions are from the same electronic state, they are expected to be also orthogonal to each other. The product of each vector with another vector, including all permutations, was then integrated. This integration resulted in no value greater than 2.92×10^{-8} . When considering precision, these numbers all can be interpreted as zero, thereby, demonstrating orthogonality. Therefore, all four eigenfunctions tested were properly normalized and orthogonal.

These four orthonormal eigenvectors were then plotted with Mathematica®. For comparison purposes, the analytical wavefunctions were also plotted on the same graph. Because these two wavefunctions coalesced so closely together, the analytical solutions were multiplied by -1 to separate the curves. Otherwise, the curves, to within plotting quality, would lay right on top of each other. Their excellent agreement can be observed in

Figure IV-1 and in Figure IV-2. Notice how the amplitudes are the same for the numerical and analytical functions. Also notice their shapes and where they cross the horizontal axis are identical.

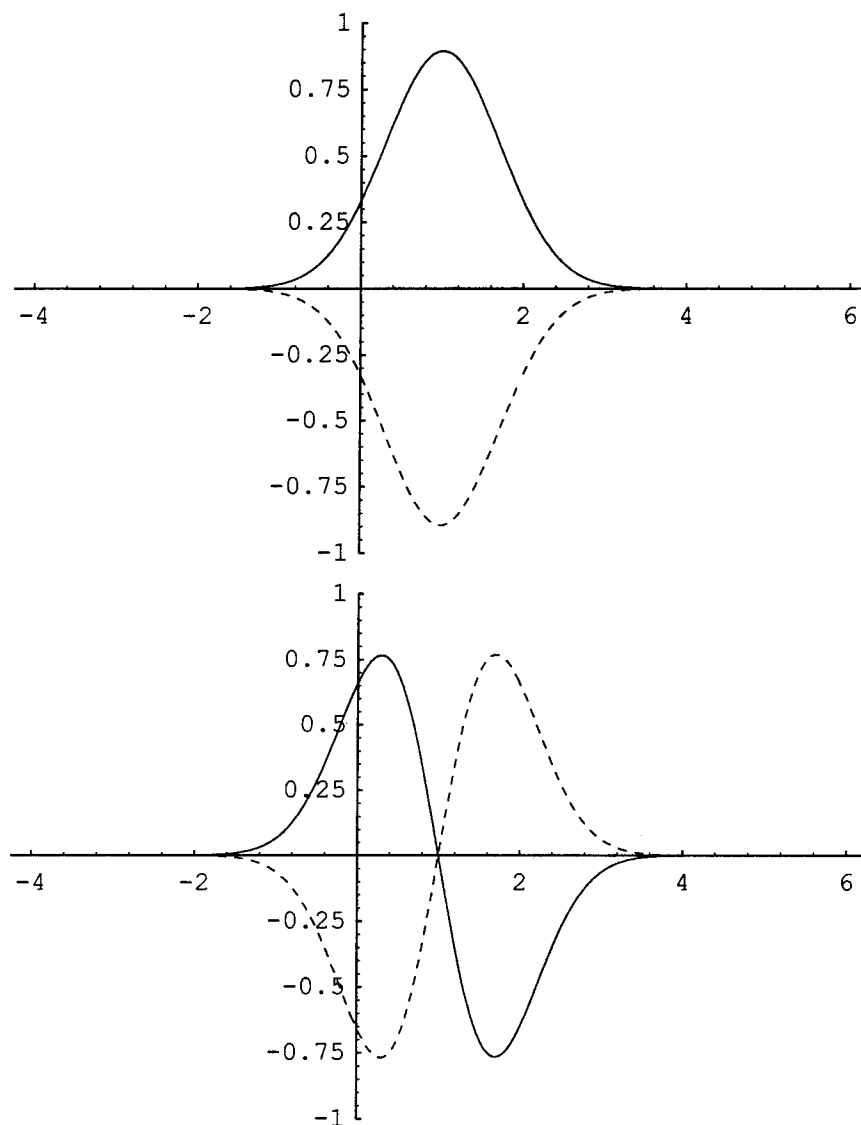


Figure IV-1. This figure shows the excellent agreement between the numerical eigenfunctions and analytical eigenfunctions of the Simple Harmonic Oscillator. Each solid curve is the numerical solution, and each dashed curve is the analytical solution. For illustrative purposes, the analytical solution has been reflected about the horizontal R_z -axis. The top curves are for the ground state ($n=0$), and the bottom curves are for the first excited state ($n=1$). Note the symmetry about $R_z=1.0$.

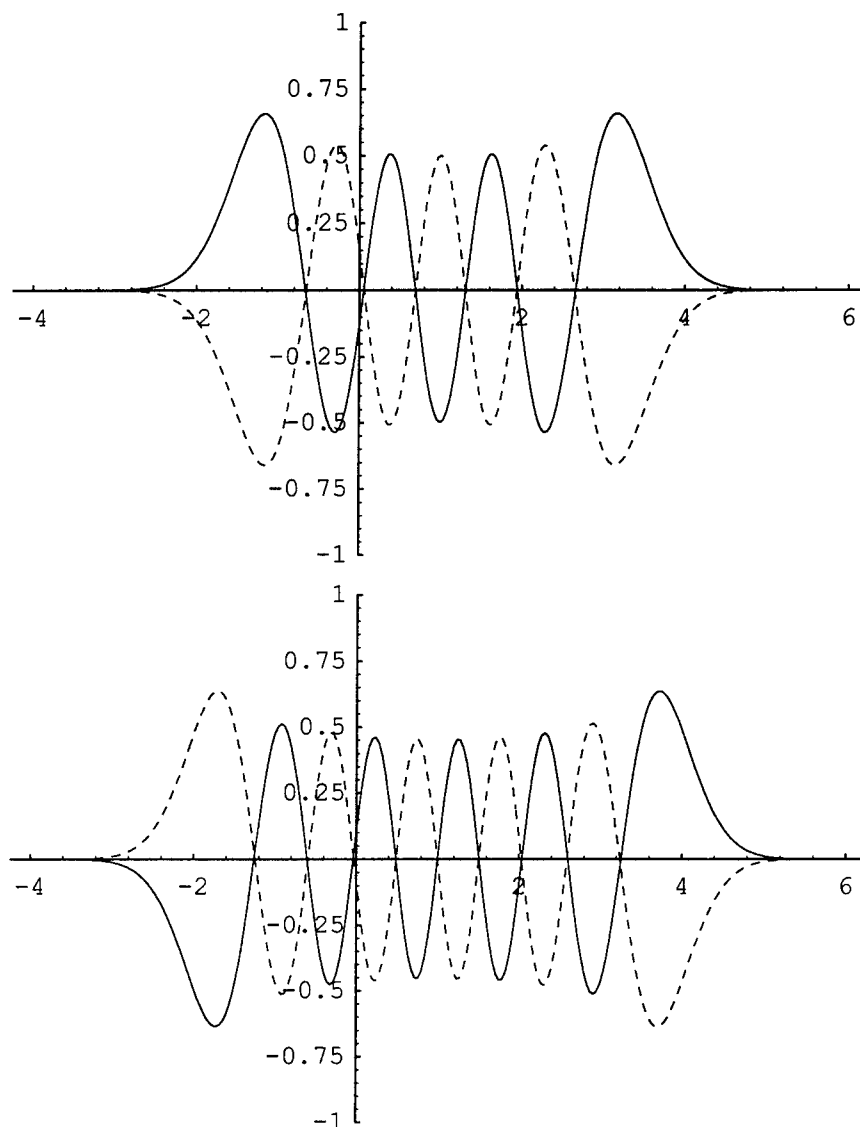


Figure IV-2. This figure also shows the excellent agreement between the numerical eigenfunctions and analytical eigenfunctions for the Simple Harmonic Oscillator. Each solid curve is the numerical solution, and each dashed curve is the analytical solution. For illustrative purposes, the analytical solution has been reflected about the horizontal R -axis. The top curves are for the state $n=6$, and the bottom curves are for the state $n=9$. Note the symmetry about $R_e=1.0$.

The Morse Anharmonic Oscillator

The Morse potential is another function with known analytical solutions. And as an added benefit, because the Morse function is such an excellent approximation of the molecular forces, this function provides a more rigorous test than the Harmonic Oscillator.

The validation process for the Morse potential proved to be more challenging than that encountered with the Harmonic Oscillator. In fact, during the validation and analysis of this function, the requirement for a subroutine to automatically correct grid placement was realized. The reason for the need for an automatic grid involves convergence issues which is discussed in the next section.

The Morse Oscillator's analytical eigenvalues and functions were calculated using Equation II-16. A dissociation energy (D_e) of 15000.0 and an anharmonicity term (a) of 6.0 was chosen for this demonstration. Again, $h/2\pi$ and the reduced mass, μ , were set to 1.0. These parameters bear no resemblance to any real molecule. But, the choice of these two parameters yields 28 bound states, which is reasonable for a molecule.

A finite element grid of 300 elements was arbitrarily chosen. The grid endpoints were located at 1.5 and 2.5, and the radius of equilibrium (R_e) was chosen to be located at 2.0.

The residuals, the difference between the numerical and analytical eigenvalues, ranged in value from 10^{-6} to 10^{-3} , except for the last two bound states which fared a little

worse. Looking at the relative errors in Table IV-2, these values ranged from 10^{-8} to 10^{-4} percent, again except for the last two states. The states very near the dissociation limit always proved more difficult to calculate. These states are on the cusp of being free states which means the grid needs to have infinite extent to model these wavefunctions.

Table IV-2. This table verifies the accuracy of the numerical solution of Schrödinger's Equation for the Morse Potential. For brevity, only selected levels of the 28 bound states are shown.

Eigenstate Level	Analytical Eigenvalue	Calculated Eigenvalue	Residual	Relative Percent Error
0	-14484.885	-14484.885	0.457E-04	0.315E-06
1	-13481.654	-13481.654	0.429E-04	0.318E-06
2	-12514.424	-12514.424	0.371E-04	0.296E-06
3	-11583.193	-11583.193	0.254E-04	0.219E-06
4	-10687.963	-10687.963	0.482E-05	0.451E-07
5	-9828.732	-9828.732	-0.273E-04	0.278E-06
...
17	-2325.967	-2325.965	-0.103E-02	0.443E-04
18	-1934.736	-1934.735	-0.106E-02	0.550E-04
19	-1579.506	-1579.504	-0.107E-02	0.680E-04
...
25	-204.123	-204.122	-0.576E-03	0.282E-03
26	-100.892	-100.892	-0.416E-03	0.412E-03
27	-33.662	-33.669	0.699E-02	0.208E-01
28	-2.431	-3.651	0.122E+01	0.502E+02
Sum of Residuals Squared			0.7439557	

The numerical wavefunctions were then developed for states 0, 1, 6, and 9 in a similar fashion as described for the harmonic wavefunctions. These four Morse wavefunctions were then tested for normalization and orthogonality.

The integration, again using Simpson's Rule, yielded normalization factors of 0.990000, 0.990001, 0.990015, and 0.989975 for states 0, 1, 6, and 9, respectively. These results can be attributed to the fact that only around 130 out of the 300 gridpoints are significant to the integral. Even though a grid was required with endpoints at 1.5 to 2.5 for convergence, these wavefunctions only exist between the points 1.85 and 2.29. The test of orthogonality yielded results not greater than 2.34×10^{-7} , except for the integrals involving state 6. These values averaged around 2.33×10^{-3} . Again, these numbers, except for state 6, can be considered zero due to precision. The integrals involving state 6 can be argued to almost vanish. Therefore, considering the approximations made with Simpson's rules and the sparse data, these functions are orthonormal.

Figure IV-3 and Figure IV-4 show the excellent agreement with the analytical solutions. Again, the analytical solutions were multiplied by -1 to separate the curves. Otherwise, they would literally lay right on top of each other. Notice the amplitudes of the analytic and numerical solutions are virtually identical. The wavefunctions also cross the horizontal exactly at the same point.

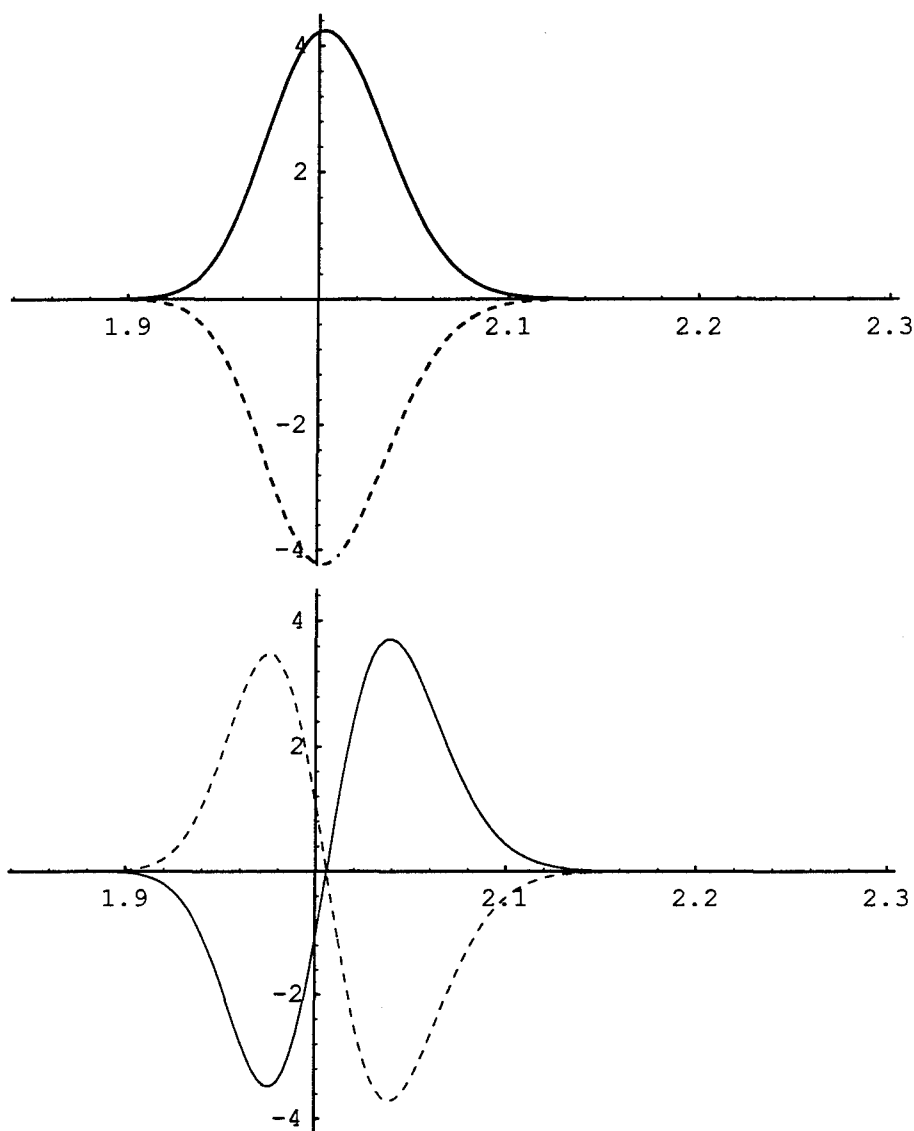


Figure IV-3. . This figure shows the excellent agreement between the numerical eigenfunctions and analytical eigenfunctions of the Morse Anharmonic Oscillator. Each solid curve is the numerical solution, and each dashed curve is the analytical solution. For illustrative purposes, the analytical solution has been reflected about the horizontal R -axis. The top curves are for the ground state ($n=0$), and the bottom curves are for the first excited state ($n=1$). Note the asymmetry about $R_e \approx 2.0$.

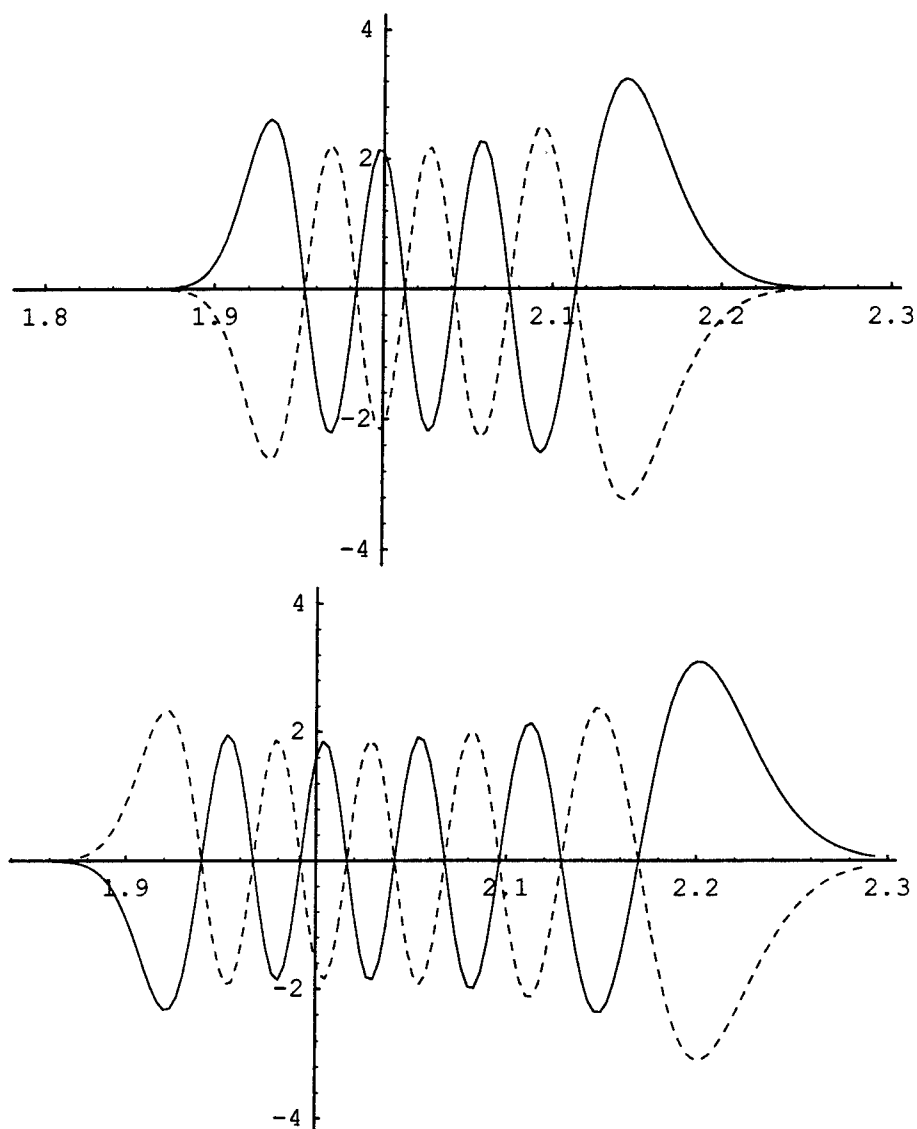


Figure IV-4. This figure also shows the excellent agreement between the numerical eigenfunctions and analytical eigenfunctions for the Morse Anharmonic Oscillator. Each solid curve is the numerical solution, and each dashed curve is the analytical solution. For illustrative purposes, the analytical solution has been reflected about the horizontal R -axis. The top curves are for the state $n=6$, and the bottom curves are for the state $n=9$. Note the asymmetry about $R_e=2.0$.

Convergence

This section details convergence testing done for the Harmonic and Morse potentials. Convergence, in the case of the method of finite elements, means that the solution should approach the “correct” answer as more elements are added to the grid, thus reducing the stepsize. However, there is a penalty for adding elements to the grid. This penalty is the cost of time. In fact, as shown later, the time required for the calculations increases cubically as the number of elements are increased.

The solutions for the Simple Harmonic Oscillator were first tested for convergence. For this model, convergence is determined by using the sum of the residuals squared as reference. This number should approach zero as the number of elements is increased.

To test for convergence, executions of *diatom* were conducted for the harmonic oscillator in a similar fashion as described earlier in the validation section. The force constant was set equal to 4.0, and $h/2\pi$ and the reduced mass were set equal to one. The grid was constructed from -5.0 to 7.0 with $R_e=1.0$. Then *diatom* was executed to see how well it predicted the analytical eigenvalues as measured by the sum of residuals squared.

Figure IV-5 shows the results of these executions as the number of elements was increased from 25 to 450. The graph clearly shows convergence, that is, as the number of

elements is increased, the solution approaches the analytical solution and the sum of the residuals squared vanishes.

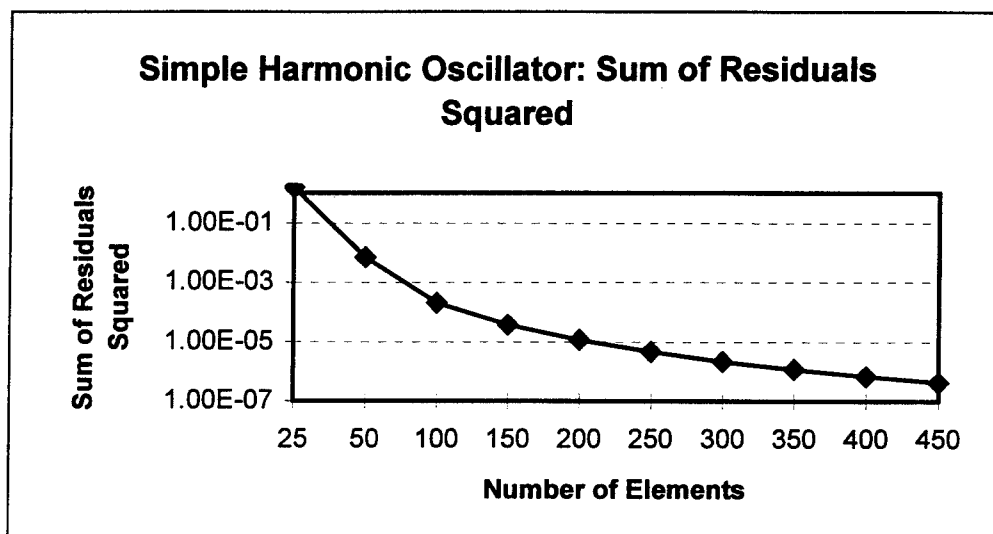


Figure IV-5. This graph demonstrates the convergence of the finite element method for the Simple Harmonic Oscillator. As the number of elements is increased, the sum of the residuals squared begins to approach zero. A plausible argument would be, given an infinite number of elements and an infinitely precise computer, the solution would converge to the analytical solution exactly. The data point at 300 corresponds to the data presented earlier in the validation section.

Next the Morse Oscillator was tested for convergence. Again, the executions were set up with $De=15000.0$ and $a=6.0$. The reduced mass and $h/2\pi$ were set to one. The radius of equilibrium (R_e) was chosen as 2.0. The left grid endpoint was set at 1.883 and the right endpoint was positioned at 4.500. At this location, the potential energy curve crosses the horizontal axis. That is, where the potential equaled zero. The thought was that the repulsive branch above zero because the solution of the free states was not wanted.

Figure IV-6 shows how the solution did not converge as expected when the number of elements was increased. The solution actually diverges. Clearly, something was wrong with the model. At the time, the reasons were unclear. In fact at this time, the method of finite elements was questioned as a reliable technique for these problems.

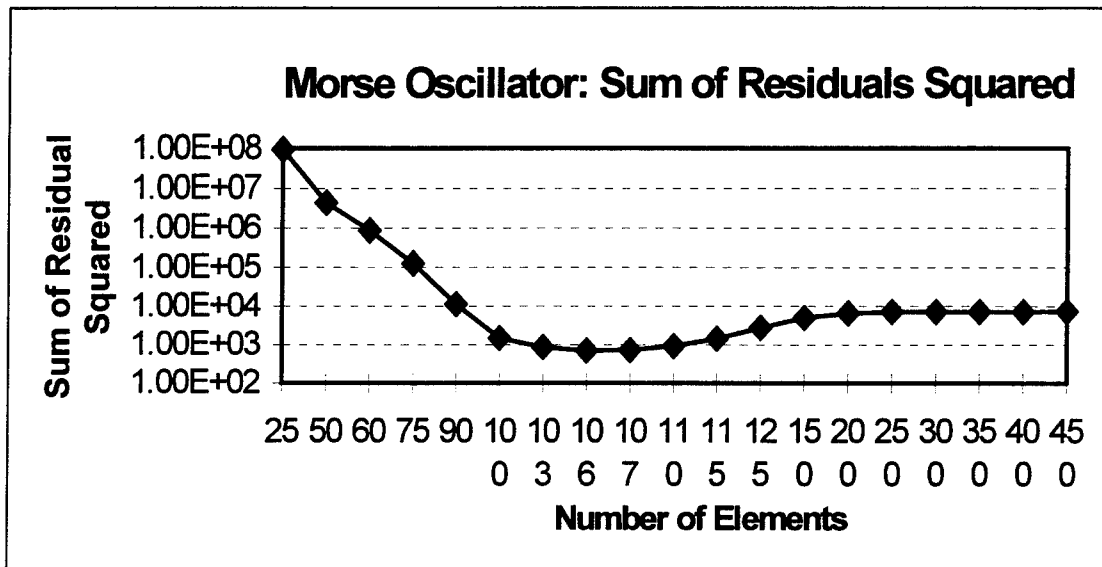


Figure IV-6. This graph shows how the solutions for the Morse potential did not converge. This graph shows how the solution diverges after the number of elements is larger than 106. Notice the scale of the Sum of Residuals Squared. The residuals diverge and round off at about 10^4 . This lack of convergence is unacceptable.

The code was then tested thoroughly because of this divergence. All of the algorithms and codes were combed through looking for errors. Then, the position of the right grid endpoint was tested to see if it affected the solutions. For this check the right gridpoint was extended towards infinity. This remedy, however, did not improve the convergence problems. Nothing seemed to work until the left grid endpoint was moved

left to 1.70 . This placement captured a large part of the repulsive branch previously thought unneeded.

Figure IV-7 shows the solution for the Morse Oscillator converging nicely to the analytic solution with this remedy. The initial lack of convergence is because the free eigenstates were not being modeled correctly.

The free states were discovered to affect the solution of the bound states. In effect, when more elements are added to the solution, more eigenstates are calculated. The rank of the **H** finite element matrix as discussed in Chapter II goes as $2(ne+1)$, where ne is the number of elements. Since this potential has only 28 bound states, any ne greater than 13 yields solutions beyond the last bound state. Therefore, to model these free states the positive repulsive branch of the potential must be included in the calculation. This requirement can be understood by realizing that within the **H** matrix, a lot of its matrix elements represent the free states. When this matrix is diagonalized, these poorly represented states will perturb the solution of the bound states.

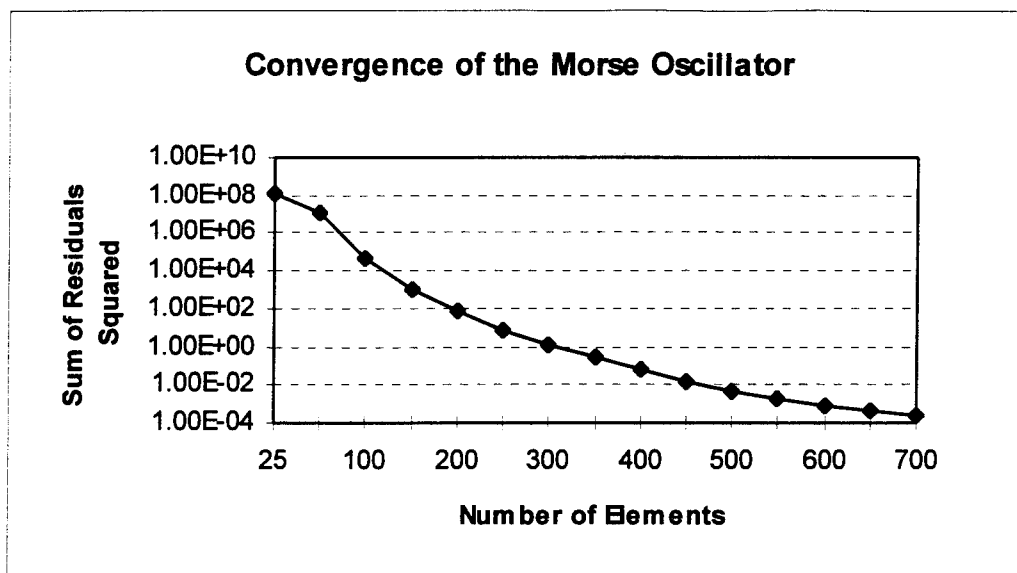


Figure IV-7. This graph shows how the finite element method does indeed converge for the Morse Oscillator. The left gridpoint was moved in from 1.883 to 1.700 capturing more of the repulsive branch. The free states interact with this part of the potential. The solution of the free states turns out to be important for the convergence of the bound states.

Further testing explored the relationship between convergence of the left grid endpoint's position. Figure IV-8 shows this relationship. As background, the number of elements for all of these solutions was fixed at 300, therefore, 702 eigenstates were being calculated. The solution can be seen to slowly converge as the left gridpoint is moved to the right. This convergence is attributed to the shrinking stepsize. At a critical point, somewhere around 1.861, the solution diverges. This divergence happens because the repulsive branch of the potential is truncated when the left endpoint is set to the right of 1.861. The free states, therefore, won't get modeled correctly. These poorly formed free states perturb the solution of the bound states.

This discovery was the genesis of the automatic grid algorithm. As the minimization routine changes parameters of the potential, the potential's repulsive branch

may swing off a previously defined grid. If this situation happens, the solutions will diverge, and the minimization routine may never find the correct solution. Therefore, an automatic system must be in place to ensure the potential is always well defined on the grid.

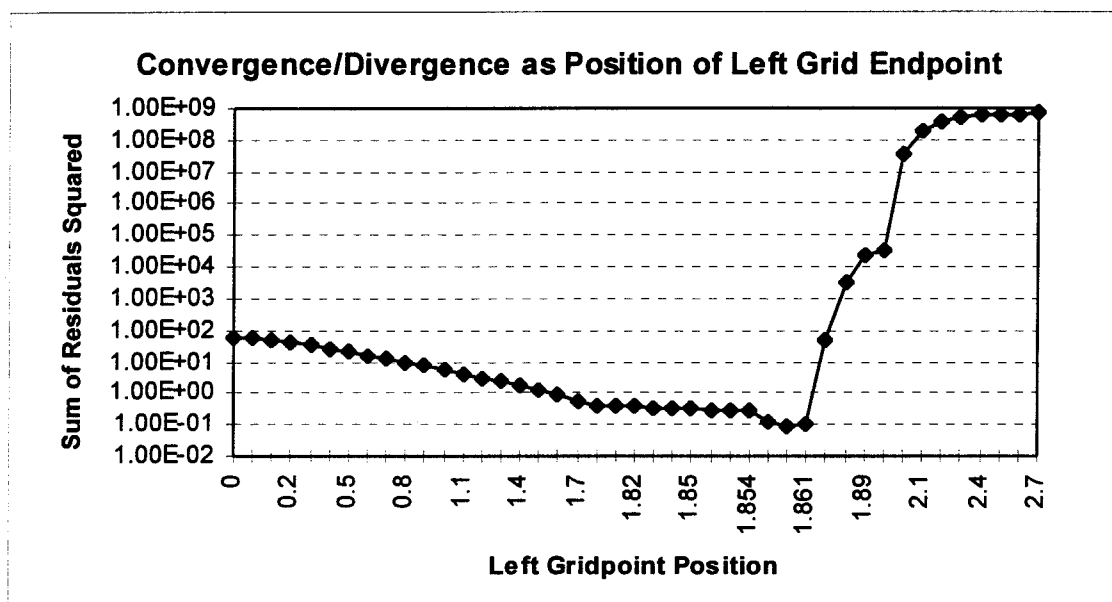


Figure IV-8. This graph shows the convergence/divergence behavior of the finite element solution of the Morse Oscillator as the left grid endpoint is moved about. The solution slowly converges as this position is moved from 0 to 1.861 . This convergence can be attributed to the decrease in the stepsize. The number of elements, which was 300, was kept constant for of these calculations. The solution then quickly diverges as the repulsive branch gets truncated. The repulsive branch is required to help model the free states. A poorly modeled free state perturbs the solutions of the bound states.

The solutions do converge given the proper position of the grid endpoints have been found. Assuming this is true, the solution should get better as the number of elements is increased. But at what cost? Recall, Equation II-33 established a relationship between the residual and the stepsize. Taking the natural logarithm of this equation yielded

$$\ln\left(\left|e(x)\right|\right) \geq \ln(c) + 4 \ln(h) \quad (\text{IV-1})$$

assuming cubic interpolating polynomials and the residual is less than one. The slope of this equation should be at least 4.

Figure IV-9 shows a convergence rate was far greater than 4. In fact, it averages around 10 for the stepsizes tested. The data used to generate this graph are identical to that used to for Figure IV-7. This curve was constructed by computing the natural logarithm of each residual and stepsize, then the slope of this curve was calculated.

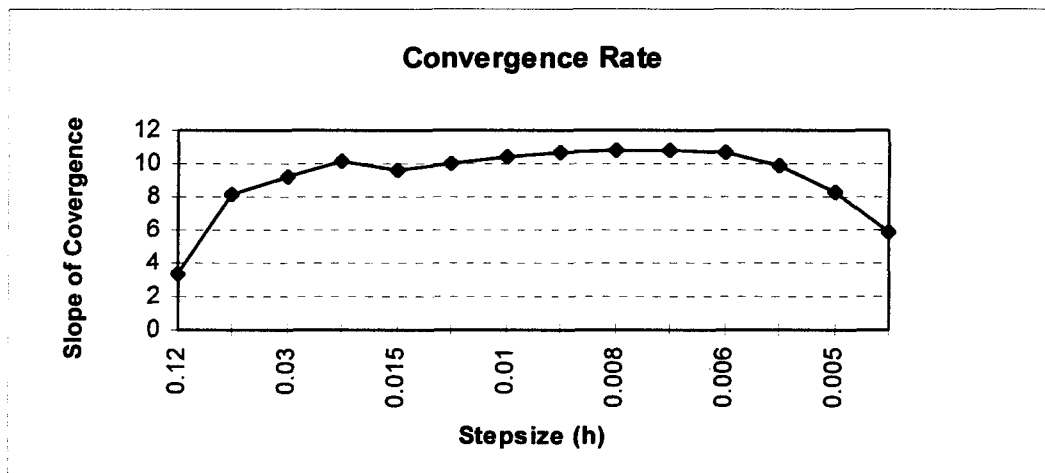


Figure IV-9. This graph shows the slope of curve formed by evaluating the natural log of the residual versus the natural log of the stepsize. In this graph, the stepsize gets smaller to the right. The slope of this curve averages about 10, far greater than 4 as predicted. These calculations are for the identical execution parameters as used to generate Figure IV-7.

However, there is a cost for increasing the number of elements. The rank of the matrices to be solved are $2(ne+1)$, where ne is the number of elements. The cost for most matrix solving algorithms is normally the rank of matrix cubed.

To find the actual cost of running *diatom*, the "user time" was recorded as a function of the number of elements. The number of elements was increased from 25 to 450 for this measurement, and the time was measured on a Sun Sparc20 ®. Figure IV-10 graphically shows these results for both the Morse and Harmonic potentials. The cost for adding elements is heavy. In fact, anything over 500 gets prohibitively slow.

This curve was then found to fit the polynomial listed below

$$\text{time} = 8.535 \times 10^{-6} ne^3 \text{ (seconds)} \quad (\text{IV-2})$$

where time has units of seconds.

This cubic relationship correlates to the cost expected when solving matrices.

This cubic result implies that very little time is spent building the matrices.

Execution Time vs Number of Elements

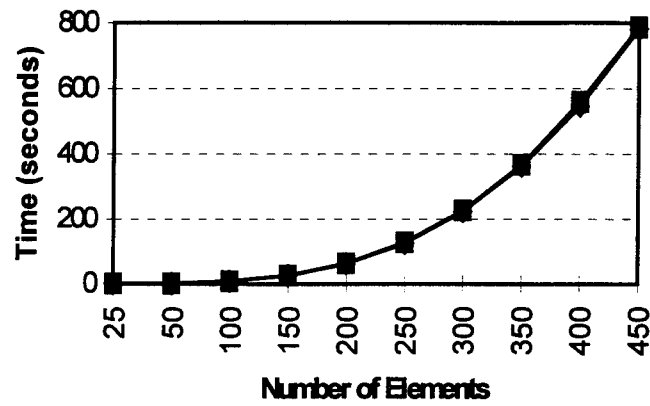


Figure IV-10. This graph illustrates the cost of adding elements. As seen previously, the more elements used for the solution, the better the answers are. However, the time for solving the finite element method goes as the number of elements cubed.

Hydrogen Molecule

In the previous section, the finite element method was shown to converge nicely for the Harmonic and Morse Oscillators. But can the full algorithm, with its non-linear minimization routine, find an unknown potential?

To test the *diatom* algorithm, a numerical (synthetic) potential for the H_2 ($X^1\Sigma_g^+$) molecule was used to calculate the vibrational eigenvalues(1, 2). This synthetic potential is an accepted approximation for the H_2 potential. A variational technique was used to calculate these eigenvalues. This calculation included 151 harmonic wavefunctions as a finite basis set for this approximation (3). Due to numerical limitations, only the energy values up to state 14 were used. Ground state H_2 has 17 bound states. These eigenvalues now represent experimental data, except this synthetic potential is exactly known unlike that of a molecule.

The vibrational eigenvalues (in atomic units) were input into *diatom* as the experimental values. The reduced mass was input as 911.422 a.u., and R_e was set at 1.424 a.u. The Morse potential was selected to see if it could model the H_2 molecule. The program *diatom* had no other information beyond this. A perfect fit was not expected.

The program *diatom* was then executed "in the blind" over six times. That is, the numerical H_2 potential described earlier was kept in confidence until all calculations were completed.

After each run, the parameter space was fine tuned as the minimization routine began to close in. At the same time, the number of elements was increased to aid the search.

The program *diatom* finally settled on an anharmonicity term of 1.0912 inverse a.u. and a dissociation energy of 0.177 Hartrees. At this point, the grid consisted of 550 elements on the interval 0.04 to 13.80 a.u. An interesting note, these grid endpoints were selected by the "smart grid" algorithm, not by the user. The reported dissociation energy is 0.1745 Hartrees (2:2467), therefore, *diatom* slightly over predicted this energy.

However, the new found potential showed excellent agreement with the numerical H_2 potential energy curve. The Morse potential, as it turns out, provides for an excellent approximation of the H_2 molecule. Figure IV-11 shows a Mathematica® plot of these two curves.

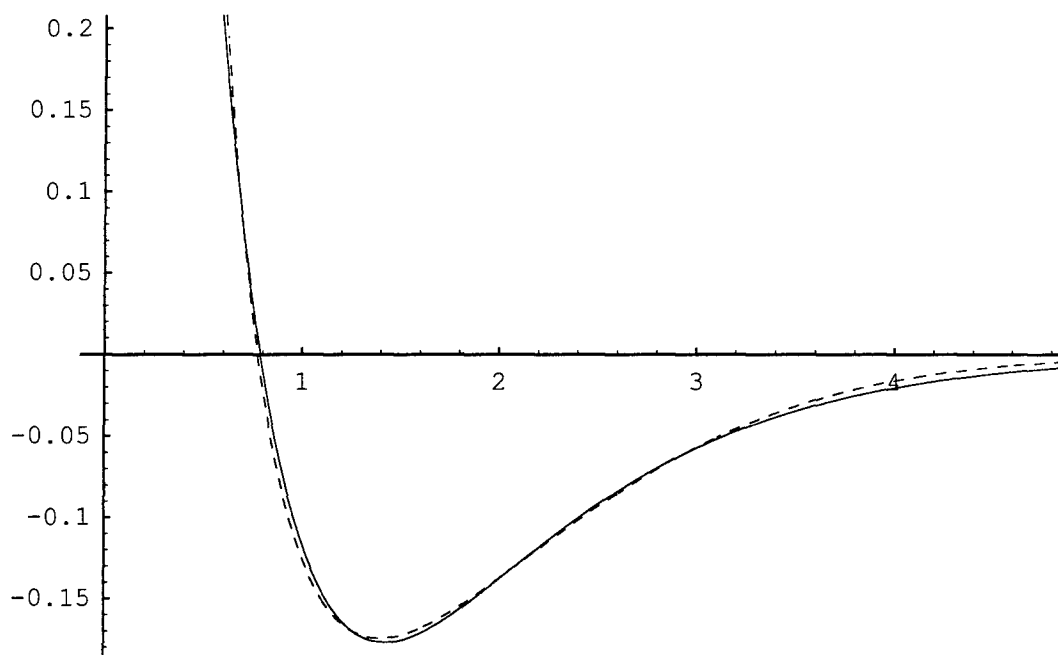


Figure IV-11. This figure shows the comparison between the potential *diatom* found for the H_2 molecule, and the numerical potential used to calculate the vibrational eigenvalues. The dashed curve is the accepted numerical H_2 molecule potential, and the solid curve is the potential found by *diatom*. The program *diatom* "found this curve in the blind." The only information it had to work with was the reduced mass of the molecule, the equilibrium position, and the vibrational eigenvalues. The Morse function, therefore, can be used to model the H_2 molecule with a great deal of accuracy, though not perfect. The units of this plot are in atomic units, therefore, the vertical axis is energy in Hartrees, and the horizontal axis is distance measured by Bohr radii.

The numerical eigenvalues also showed excellent agreement. The program *diatom* attempts to fit all of the eigenvalues simultaneously. This process means it tries just as hard to fit the upper states as the lower states, but not always with success. For the first 11 states, the relative error was less than 10%, and for the bottom five levels it's less than 2%. From this table, it is clear the Hydrogen molecule can't be exactly be modeled

by the Morse function because in some places it under predicts, and others it over predicts. The residuals do not follow a systematic pattern.

Table IV-3. This table shows the accuracy of diatom's predictions for the H₂ molecule. The accepted values are the eigenvalues calculated using the accepted potential curve. The units of these energies are in Hartrees.

Energy Level	Accepted Eigenvalues	Predicted Eigenvalues	Residual	Percent Relative Error
0	-0.165	-0.166	0.187E-02	0.114E+01
1	-0.146	-0.146	0.641E-03	0.440E+00
2	-0.128	-0.127	-0.362E-03	0.283E+00
3	-0.111	-0.110	-0.111E-02	0.999E+00
4	-0.950E-01	-0.935E-01	-0.158E-02	0.166E+01
5	-0.803E-01	-0.785E-01	-0.178E-02	0.222E+01
6	-0.665E-01	-0.648E-01	-0.172E-02	0.258E+01
7	-0.539E-01	-0.525E-01	-0.140E-02	0.260E+01
8	-0.423E-01	-0.414E-01	-0.862E-03	0.204E+01
9	-0.318E-01	-0.317E-01	-0.169E-03	0.532E+00
10	-0.226E-01	-0.232E-01	0.620E-03	0.274E+01
11	-0.147E-01	-0.161E-01	0.140E-02	0.951E+01
12	-0.823E-02	-0.102E-01	0.202E-02	0.245E+02
13	-0.345E-02	-0.573E-02	0.228E-02	0.660E+02
14	-0.630E-03	-0.251E-02	0.188E-02	0.299E+03

Conclusion

In conclusion, the program *diatom* and the method of finite element was proven to provide credible solutions of Schrödinger's Equation. These solutions included wavefunctions, energy eigenvalues, and potential curves for diatomic molecules.

The numerical wavefunctions of the Morse and Harmonic oscillators were shown to be orthonormal. The relative error of the eigenvalues was typically on the order of 10^{-6} and 10^{-3} percent for the Morse and Harmonic functions, respectively. Convergence and cost of convergence was also discussed.

The H_2 molecule was then used to show the model could be used to find an "unknown" potential curve. The model predicted an anharmonicity of 1.0912 inverse a.u. and a dissociation energy of 0.177 Hartrees for the ground state of H_2 . The graphical comparison of the accepted potential energy curve and the predicted curve showed excellent agreement.

V . Conclusion

Summary

The method of finite elements was proven to be a viable technique for solving Schrödinger's Equation for the vibrational states of diatomic molecules. The calculation of Franck-Condon Factors was explained using experimental spectroscopic data in conjunction with four computer programs (*efit*, *dunham*, *diatom*, *fcf*). The focus of this research, however, centered on the validation of one of those programs, *diatom*.

The program, *diatom*, requires as input the experimental vibrational eigenvalues for each electronic state. Then using the method of finite elements, the program solves Schrödinger's Equation and computes the eigenvalues. These eigenvalues are then compared to the experimental values to establish how well the selected potential energy model resembles the unknown real potential surface. The adequacy of this selected potential model is measured by the sum of the residuals squared. A non-linear minimization routine then modifies the parameters of the potential energy model to reduce this value, the sum of the residuals squared. This process is repeated until the sum of residuals squared has been minimized identifying the optimal parameter choice. After the optimal potential model has been isolated, the vibrational eigenfunctions are then

calculated. The vibrational eigenfunctions from two different electronic states are then used to calculate the Franck-Condon Factors.

To validate the program *diatom*, the Simple Harmonic and Morse Anharmonic Oscillators were exploited for their known analytical solutions. The relative error of the computational eigenvalues was typically on the order of 10^{-6} and 10^{-3} percent for the Morse and Harmonic functions, respectively. The numerical wavefunctions of these oscillators were shown to be orthonormal, and matched the analytical wavefunctions extremely well when plotted.

Next, to demonstrate the model could indeed be used to isolate an optimal potential surface, the H_2 molecule was selected for the test. The H_2 molecule is the simplest and one of the most studied molecules, lending itself for an this test ideally. The vibrational eigenvalues for the electronic ground state were generated using an accepted potential surface for the H_2 molecule. These eigenvalues were then input into the model. Using a Morse potential model, *diatom* isolated the optimal surface with an anharmonicity term of 1.0912 inverse a.u. and a dissociation energy of 0.177 Hartrees. The graphical comparison of the accepted potential energy surface and predicted surface showed excellent agreement.

Recommendations

In summary, this numerical technique has proved to be an excellent method for finding unknown potential surfaces of real molecules. However, before this method can be shown to provide solutions which equal or better the RKR-IPA approach, more testing needs to be accomplished. The following suggestions outlines areas for additional research and improvements:

- Perform extensive testing of the code on more complicated molecules to demonstrate the utility of this numerical approach. Preferably, a molecule such as PbO or some other would be chosen which has a large empirical knowledge base, and has been similarly solved with the RKR method. The results of these studies should be published.
- Validate the code for a real molecule (such as PbO) at the Franck-Condon Factor level. A molecule's wavefunctions and potential energy curve can not be directly observed. Only the spectral locations and intensities of the molecule's transitions can be directly observed. Experimental Franck-Condon Factors can be obtained by removing the population influence of the transition intensities, and then normalizing each intensity. The normalization factor is the sum of the intensities after the population influence has been removed. Comparisons at this level mark the code's final test for validity.

- Add more potential functions to the menu the user can choose from. This list now only includes the Simple Harmonic Oscillator, Morse Anharmonic Oscillator, Lennard-Jones, and Mie potentials. This numerical technique lends itself very nicely to very sophisticated potential functions which may model the physics better.
- Replace the non-linear minimization routine currently used with a faster and more efficient routine. The current routine is an excellent choice for a turbulent parameter space with lots of tiny local minima. However, this research suggest that these parameter spaces are fairly smooth and the existence of only one minimum. This enhancement could dramatically decrease run time.
- Integrate all four codes (*efit*, *dunham*, *diatom*, *fcf*) into one seamless code. This modification would make the work required of the user simpler. In this way, the user would only have to manage one input file. This enhancement is necessary before this code is distributed in any way.
- Consider replacing the IMSL® math routines with non-proprietary code. This modification would eliminate any portability issues which may arise.

Bibliography

Chapter I

- ¹ Verdeyen, Joseph T. Laser Electronics. Englewood Cliffs: Prentice Hall, 1995.
- ² Rutger, Lyle L. Numerical Methods for the Preparation of Potential Energy Curves of Diatomic Molecules. MS Thesis. Air Force Institute of Technology, Wright-Patterson Air Force Base, OH, 1983
- ³ Pow, Joseph J.. The Development of Computer Routines to Perform a Comprehensive Analysis of Spectroscopic Data from Diatomic Molecules. MS Thesis Air Force Institute of Technology, Wright-Patterson Air Force Base, OH, 1983
- ⁴ Brasure, LeAnn D. Calculation of Franck-Condon Factors for Diatomic Molecules. MS Thesis Air Force Institute of Technology. Wright-Patterson Air Force Base, OH, 1985
- ⁵ Scheingraber, H. and C. R. Vidal. "Determination of Diatomic Molecular Constants Using an Inverted Perturbation Approach, Application to the $A \Sigma_{\mu}^{+} - X_g^{+}$ System of Mg_2 ," Journal of Molecular Spectroscopy, 65: 46-64 (1977).
- ⁶ Zare, R. N., A. L. Schmeltekopf, W. J. Harrop, and D. L. Albritton. "A Direct Approach for the Reduction of Diatomic Spectra to Molecular Constants for the Construction of RKR Potentials," Journal of Molecular Spectroscopy, 46: 37-66 (1973).
- ⁷ Wells, Bryan H., E. Brian Smith, and Richard N. Zare. "The Stability of the RKR Inversion Procedure to Errors in the Spectroscopic Data: Origin of the Inner-Wall Ripple," Chemical Physics Letters, 99: 244-249 (August 1983).
- ⁸ Tellinghuisen, Joel and Stuart D. Henderson. "The Use of Morse-RKR Curves in Diatomic Calculations," Chemical Physics Letters, 91: 447-451 (October 1982).
- ⁹ Morse, Philip M. "Diatomic Molecules According to the Wave Mechanics. II. Vibrational Levels," Physical Review, 34: 57-63 (July 1929)
- ¹⁰ Ostdiek, Paul H. Computer Modeling of Vibrational Energy Levels of Potential Laser Candidates. MS Thesis. Air Force Institute of Technology, Wright-Patterson Air Force Base, OH, 1984

Chapter II

- ¹ Verdeyen, Joseph Laser Electronics. Englewood Cliffs: Prentice Hall, 1995
- ² Wolf, Paul J. Atomic and Molecular Spectroscopy Lecture Notes. Air Force Institute of Technology, Wright-Patterson Air Force Base, Spring 1995.
- ³ Struve, Walter S. Fundamentals of Molecular Spectroscopy. New York: John Wiley & Sons, 1989.
- ⁵ Born, M. And R. Oppenheimer "Zur Quantentheorie der Molekeln," Annalen Der Physik V. Folge 84, 1927
- ⁶ Steinfeld, Jeffrey I. Molecules and Radiation: An Introduction to Modern Molecular Spectroscopy. New York: Harper & Row, 1981.
- ⁸ Anderson, Elmer E. Modern Physics and Quatum Mechanics. Philadelphia: W.B. Saunders Co., 1971.
- ⁹ Feagin, James M. Quantum Methods with Mathematica®. New York: Springer Verlag, 1994
- ¹⁰ Morse, Phillip M. "Diatomic Molecules According to the Wave Mechanics. II. Vibration Levels," Physical Review, Vol. 34, 1929
- ¹¹ Morse, Phillip M. "Diatomic Molecules According to the Wave Mechanics. II. Vibration Levels," Physical Review, Vol. 34, 1929
- ¹² Arfken, George Mathematical Methods for Physicists. San Diego: Academic Press, Inc. 1985
- ¹³ Atkins, Peter W. Quanta: A Handbook of Concepts. London: Oxford University Press, 1974
- ¹⁴ Pepper, Darrell W. And Juan C. Heinrich The Finite Element Method: Basic Concepts and Applications. Washington: Hemisphere Publishing Corp., 1992
- ¹⁵ Ostdiek, Paul H. Computer Modeling of Vibrational Energy Levels of Potential Laser Candidates. MS Thesis, Air Force Institute of Technology, Wright-Patterson Air Force Base, 1984
- ¹⁶ Rao, S.S. The Finite Element Method in Engineering New York: Pergamon Press, 1982
- ¹⁷ Couillette, David Finite Element Techniques in Applied Science, Lecture Notes, Summer 1995

Chapter III

¹ Dunham, J. L. "The Energy Levels of a Rotating Vibrator," Physical Review, 41: 721-731 (May 1932)

² Ostdiek, Paul H. Computer Modeling of Vibrational Energy Levels of Potential Laser Candidates. MS Thesis, Air Force Institute of Technology, Wright-Patterson Air Force Base, 1984

³ Struve, Walter S. Fundamentals of Molecular Spectroscopy. New York: John Wiley & Sons, 1989

⁴ Atkins, Peter W. Quanta: a Handbook of Concepts Oxford: Clarendon Press, 1974

⁵ Pearson, Carl E. Private Notes on Optimization Program *Min*, University of Washington, 1992

⁶ User's Manual, IMSL Math/Library® FORTRAN Subroutines for Mathematical Applications, Version 1.1, 1989

Vita

Matthew C. Smitham was born in Bellingham, ~~Washington 1964~~. He graduated from Sehome High School, Bellingham, Washington in 1985. He was admitted to the University of Washington and enrolled in the Air Force Reserve Officer Training Corps (ROTC) that same year. Upon graduation in 1989 he was awarded a Bachelor of Science in Physics and commissioned a Second Lieutenant in the United States Air Force. His first principle assignment was as a scientific analyst for the Air Force Electronic Warfare Center located at Kelly AFB, Texas. There he analyzed, measured, and modeled infrared signatures of US aircraft to determine the vulnerability of US aircraft against infrared guided missiles. This research was used for operations including Desert Storm, mission planning and tactics development, and acquisitional support. In 1994 he was awarded the Air Force Commendation Medal for Meritorious Service. He enrolled in the Air Force Institute of Technology in the spring of 1994 to obtain his Masters in Physics. Upon graduation he will be assigned to the Phillips Laboratory at Hanscom AFB, Massachusetts.

~~Present Address:~~

~~311 West Forest St.~~

~~Bellingham, Washington 98201~~

REPORT DOCUMENTATION PAGE			Form Approved OMB No. 0704-0188	
Public reporting burden for this collection of information is estimated to average 1 hour per response, including the time for reviewing instructions, searching existing data sources, gathering and maintaining the data needed, and completing and reviewing the collection of information. Send comments regarding this burden estimate or any other aspect of this collection of information, including suggestions for reducing this burden, to Washington Headquarters Services, Directorate for Information Operations and Reports, 1215 Jefferson Davis Highway, Suite 1204, Arlington, VA 22202-4302, and to the Office of Management and Budget, Paperwork Reduction Project (0704-0188), Washington, DC 20503.				
1. AGENCY USE ONLY (Leave blank)	2. REPORT DATE December 1995	3. REPORT TYPE AND DATES COVERED Master's Thesis		
4. TITLE AND SUBTITLE IDENTIFICATION OF MOLECULAR LASER TRANSITIONS USING THE FINITE ELEMENT METHOD		5. FUNDING NUMBERS		
6. AUTHOR(S) Matthew C. Smitham, Capt, USAF				
7. PERFORMING ORGANIZATION NAME(S) AND ADDRESS(ES) Air Force Institute of Technology/ENP 2950 P Street Wright-Patterson Air Force Base OH 45431		8. PERFORMING ORGANIZATION REPORT NUMBER AFIT/GAP/ENP/95D-14		
9. SPONSORING / MONITORING AGENCY NAME(S) AND ADDRESS(ES) Phillips Laboratory/LIDB (Dr Ernest A. Dorko) 3550 Aberdeen Ave SE Kirtland Air Force Base NM 87117-5776		10. SPONSORING / MONITORING AGENCY REPORT NUMBER		
11. SUPPLEMENTARY NOTES				
12a. DISTRIBUTION / AVAILABILITY STATEMENT Approved For Public Release; Distribution Unlimited		12b. DISTRIBUTION CODE		
13. ABSTRACT (Maximum 200 words) This thesis is a continuation of a previous effort which developed a finite element solution of Schrödinger's Equation. Identification of laser transition rates can be obtained by solving Schrödinger's Equation for diatomic molecules using the finite elements method. Experimental vibrational eigenvalues for a given electronic state are used to determine the molecular potential surface which yields the closest numerical result. A non-linear minimization routine is used to hunt for this surface by adjusting parameters of energy functions such as the Harmonic, Morse, Lennard-Jones, and Mie potentials. The eigenvalues from these solutions are then compared to the experimental values. Through this iterative process, the best potential surface is isolated. Franck-Condon factors are then computed with the numerical eigenfunctions from two different potential surfaces found in this way. This numerical technique was able to isolate potential surfaces whose eigenvalue solutions had relative errors better than 10^{-3} and 10^{-6} percent when compared to the analytical solutions of the Harmonic and Morse oscillators, respectively. Comparisons of the wavefunctions also yielded excellent agreement. Initial work with H_2 ($X^1\Sigma_g^+$) verifies the lower eigenstates can be approximated by the Morse potential with an anharmonicity term of 1.0912 inverse a.u. and a dissociation energy of 0.177 Hartrees.				
14. SUBJECT TERMS Laser, Diatomic, Molecules, Spectroscopy			15. NUMBER OF PAGES 114	
			16. PRICE CODE	
17. SECURITY CLASSIFICATION OF REPORT UNCLASSIFIED	18. SECURITY CLASSIFICATION OF THIS PAGE UNCLASSIFIED	19. SECURITY CLASSIFICATION OF ABSTRACT UNCLASSIFIED	20. LIMITATION OF ABSTRACT UL	